Characterization and Fabrication of Synthetic Rough Surfaces for Acoustical Scale-Model Experiments

JASON E. SUMMERS
RAYMOND J. SOUKUP
ROBERT F. GRAGG

Acoustic Systems Branch
Acoustics Division

August 5, 2005

REPORT DOCUMENTATION PAGE

1. REPORT DATE *(DD-MM-YYYY)*	2. REPORT TYPE	3. DATES COVERED *(From - To)*
05-08-2005	Memorandum Report	

4. TITLE AND SUBTITLE

Characterization and Fabrication of Synthetic Rough Surfaces for Acoustical Scale-Model Experiments

5a. CONTRACT NUMBER

5b. GRANT NUMBER

5c. PROGRAM ELEMENT NUMBER

6. AUTHOR(S)

Jason E. Summers, Raymond J. Soukup, and Robert F. Gragg

5d. PROJECT NUMBER

5e. TASK NUMBER

5f. WORK UNIT NUMBER

7. PERFORMING ORGANIZATION NAME(S) AND ADDRESS(ES)

Naval Research Laboratory, Code 7140
4555 Overlook Avenue, SW
Washington, DC 20375-5320

8. PERFORMING ORGANIZATION REPORT NUMBER

NRL/MR-MM/7140--05-8871

9. SPONSORING / MONITORING AGENCY NAME(S) AND ADDRESS(ES)

Office of Naval Research
800 North Quincy Street
Arlington, VA 22217-5660

10. SPONSOR / MONITOR'S ACRONYM(S)

11. SPONSOR / MONITOR'S REPORT NUMBER(S)

12. DISTRIBUTION / AVAILABILITY STATEMENT

Approved for public release; distribution is unlimited.

13. SUPPLEMENTARY NOTES

14. ABSTRACT

Diverse aspects of stochastic processes, time-series analysis and fractal geometry are applied to the problem of characterizing and fabricating scale-model representations of the ocean bottom for acoustical analysis. As these physical models of rough surfaces are of finite size and manufacturing resolution, they are properly treated as examples of band-limited fractional Brownian motion (FBM), a type of approximately self-affine fractal. A novel formalism for the generation and characterization of FBM surfaces is developed, and the high- and low-wavenumber bandwidth restrictions are described analytically and presented visually. Specific applications involving acoustic tank experiments for verifying the predictions of rough surface scattering theories are described. MATLAB code for creating and validating mathematical representations of FBM surfaces is provided.

15. SUBJECT TERMS

Acoustic scattering; Rough-surface scattering; Physical modeling; Power-law roughness spectrum; Fractional brownian motion; Computer-aided manufacturing

16. SECURITY CLASSIFICATION OF:			17. LIMITATION OF ABSTRACT	18. NUMBER OF PAGES	19a. NAME OF RESPONSIBLE PERSON
a. REPORT	**b. ABSTRACT**	**c. THIS PAGE**	UL	48	Jason E. Summers
Unclassified	Unclassified	Unclassified			**19b. TELEPHONE NUMBER** *(include area code)* (202) 404-4813

Standard Form 298 (Rev. 8-98)
Prescribed by ANSI Std. Z39.18

Contents

CHARACTERIZATION AND FABRICATION OF SYNTHETIC ROUGH SURFACES FOR ACOUSTICAL SCALE-MODEL EXPERIMENTS

I.   INTRODUCTION

The study of energy scattered from rough surfaces spans a number of disciplines, among them those involving either sound or electromagnetic waves. Within the field of acoustics, rough-surface scattering impacts sound fields in rooms, noise in urban environments, and acoustic boundary interaction in the ocean. Ocean acoustics, in particular, utilizes theories of scattering from rough surfaces to characterize the interaction of sound with the ocean surface (air-water interface) and bottom (water-bottom interface and subsurface layers). For characterizing the performance of sonar systems, a number of theories have been applied to cover a wide range of frequencies and the entire range of scattering geometries in three dimensions. Some theories require limitations on the roughness, such as perturbation theory or small-slope theory [1, 2]; others place limitations on the geoacoustic parameters of an ocean bottom, such as wedge assemblage [3, 4]. While rough surfaces of ocean bottoms may involve topographical variations arising from either geological processes or discrete objects (such as shells), here discussion focuses on rough surfaces of purely geological origin.

This report describes a portion of a larger effort to characterize wave-field scattering by rough surfaces found in nature—specifically the scattering of acoustic fields by rough ocean bottoms.

Characterization of acoustic scattering by rough ocean bottoms requires not only devising an adequate mathematical/physical theory of rough-surface scattering and implementing it in software (see [2]), but also conducting an exhaustive verification by comparison with scattering data from experimental measurements or numerical simulations. However, both of these methods for verification of model predictions have practical and technical limitations. The scarcity of adequate data on ocean-bottom properties and the consequent inability to conduct systematic studies of the dependence of ocean-bottom scattering strength on a roughness parameter, such as spectral exponent (see Sec. II B) make verification using scattering data taken from natural sea floors impractical. Numerical modeling (e.g., finite-element and boundary-element methods) also has practical limitations. While it has been successfully applied to two-dimensional scattering from surfaces with stochastic roughness that varies in one dimension only, three-dimensional scattering from surfaces with stochastic roughness that varies in two dimensions can present significant difficulties. To circumvent these limitations, small-scale physical models of rough ocean bottoms have been manufactured at sizes manageable for use in an acoustic tank facility and verification has been conducted using data taken in the laboratory at appropriately scaled-up frequencies. Such models can be used to investigate theoretical predictions relating to both roughness parameters and geoacoustic parameters such as compressional and shear speeds/attenuations (see Ref. 5 and references therein). In manufacturing these small-scale experimental models, no attempt has been made to recreate any actual geophysical region in miniature. Rather, ocean-bottom topography is described using the mathematics of self-affine stochastic fractals.

Scattering theories applied in underwater acoustics fall into two categories: those involving a stochastic description of the rough surface and those treating the rough surface deterministically. In this report, stochastic rough surfaces are discussed exclusively. However, the stochastic rough surface is an abstraction; statistical properties of rough surfaces are more properly regarded not as properties of individual surfaces

1

but as properties of the ensemble of rough surfaces that are realizations of a particular random process. Individual realizations are, when considered in isolation, deterministic. Therefore, physical models created to represent stochastic ocean bottoms and test stochastic scattering theories can also be used for testing deterministic scattering theories.

Choosing to verify scattering theories by means of physical scale models based on fractal geometry requires that three tasks be achieved: (1) understanding the application of the abstract mathematics of fractal geometry to the description of surface topography, (2) incorporating into fractal models recent results that quantify the effects of representing unbounded self-affine fractal surfaces as bounded, discretely sampled objects, and (3) developing or adapting the algorithms necessary to fabricate physical realizations of fractals using a modern computer-numerically controlled milling machine. The information that was found to be essential for success in these three tasks has been summarized in this report. The implementation of those concepts and techniques needed for the manufacture of random rough surfaces are illustrated by accompanying MATLAB code. This code allows users to numerically generate rough surfaces that are two-dimensional realizations of band-limited fractional Brownian motion and allows for such surfaces to be characterized in terms of statistical and fractal metrics.

This report is grouped into two primary sections: Characterization of Rough Surfaces and Fabrication of Rough Surfaces. In the first of these sections, a number of disparate elements are brought together in order to provide a mathematical description of rough surfaces as both random processes and stochastic fractals. A parameter study (portions of which are shown in the Appendix A) illustrates the relationship between the appearance of rough surfaces and their roughness parameters. The final portion of the first section relates the preceding theoretical development to real ocean bottoms by considering both how roughness parameters affect scattering and the range of roughness parameters observed in the ocean. The second section describes how physical models of the surfaces described in the first section can be computationally generated and then physically fabricated with the use of computer-aided-manufacturing equipment, and how the accuracy of the resulting realization can be tested. The report concludes with a summary of the material presented. Appendices B and C give further details of the algorithms used for the computational generation and physical fabrication of rough surfaces, including descriptions of MATLAB software tools included on the CD-ROM with this report. Abbreviations and symbols are defined in a glossary located at the end of this report. Numerical quantities are given in SI (MKS) units exclusively.

While the primary goal of this work is to bring together concepts from disparate disciplines, throughout the report a number of new concepts are introduced. In particular, the recent concept of approximately self-affine surfaces is applied to numerical generation and physical fabrication of realizations of random rough surfaces. The high- and low-k bandwidth restrictions inherently imposed by these processes are related to their effects on the properties of surfaces both as characterized by fractal mathematics and observed visually.

II. CHARACTERIZATION OF ROUGH SURFACES

In this section, a consistent description of rough-surface topography is developed through a series of definitions. Rough surfaces are described first as infinite-extent realizations of random processes. In Sec. II B each such process is characterized by a power-spectral density (PSD), in particular, a PSD that follows a power-law form over some portion of the spectrum. A parallel description of rough-surface topography in terms of stochastic fractals is developed in Sec. II C and related to characterization in terms of PSD. Particular attention in both descriptions of surface roughness is given to surfaces having cutoff power-law PSD for which the power-law behavior is restricted in bandwidth at one or both frequency extremum. In Sec. II D, realizations of stochastic rough surfaces are generated to provide an intuitive presentation of the

effects of surface-roughness parameters on the appearance of rough surfaces.

A. Statistics of Rough-Surface Topography

A rough surface is described by its topography $z(\mathbf{r})$, which is the height of the surface above a plane containing position vector $\mathbf{r}$ having Cartesian components (x, y). The topography is given by the mapping $\{z(\mathbf{r}) : \mathbf{r} \in \mathbb{R}^2\}$ which defines a surface in $\mathbb{R}^3$ (it is assumed here that the surface topography is single valued). In this initial discussion, rough surfaces are considered to be of infinite extent and defined for all values of $\mathbf{r}$, (i.e., 'continuous' in signal-processing terminology), as the expression for the mapping from $\mathbb{R}^2$ implies. In practice, $z(\mathbf{r})$ is defined over a finite set of discrete points having finite physical dimensions. The consequences of this will be addressed in Sec. III A 1.

Geomorphological rough surfaces are, by necessity [6], modeled as realizations of random processes such that the ensemble of realizations $\{z\}$ of a particular random process is described by the probability density function (PDF) of surface height $f_z(\zeta)$ where ζ is the set of possible surface heights. In the following discussion, it is initially assumed that the random process possesses certain statistical attributes (see, e.g., Ref. 7, pp. 23–27): homogeneity (stationarity or translational invariance), isotropy (rotational invariance), and ergodicity (equivalence of spatial averages over a single realization to ensemble averages).

Given an appropriate choice of the reference plane from which z is measured, the mean height of the surface $\langle z \rangle$ is zero

$$\langle z \rangle = \int_{-\infty}^{\infty} \zeta f_z(\zeta) d\zeta = 0 , \tag{1}$$

where $\langle \cdot \rangle$ is an expectation operator. The assumption of ergodicity allows this operator to be interpreted either as a spatial, $\langle \cdot \rangle_s$, or ensemble, $\langle \cdot \rangle_e$, average. Zero-mean height can be alternatively achieved by modeling the topography as the sum of two functions $z(\mathbf{r}) + z_0(\mathbf{r})$ where $z(\mathbf{r})$ is the stochastic small-scale roughness and $z_0(\mathbf{r})$ is the deterministic large-scale roughness [8]. Thus, $z_0(\mathbf{r})$ effectively detrends the data and ensures $\langle z \rangle = 0$. The root-mean-square (RMS) surface roughness (sometimes termed interface width) σ is given by the standard deviation of $f_z(\zeta)$

$$\sigma = \sqrt{\langle z^2 \rangle} = \sqrt{\int_{-\infty}^{\infty} \zeta^2 f_z(\zeta) d\zeta} . \tag{2}$$

In many cases the height PDF of real random rough surfaces is Gaussian in form:

$$f_z(\zeta) = \frac{1}{\sigma\sqrt{2\pi}} \exp\left(-\frac{\zeta^2}{2\sigma^2}\right) . \tag{3}$$

This is a consequence of the central-limit theorem, which predicts that the PDF $f_\Xi(\zeta)$ of the sum of n independent identically distributed random variables, $\Xi = \sum_{i=1}^{n} \Lambda_i$, tends toward Gaussian form as $n \to \infty$, provided that Λ_i have finite mean and finite variance.

Surfaces having identical PDFs are distinguished from one another by higher-order statistical descriptors, which may be expressed in either spatial or spectral domains. In particular, Gaussian surfaces (those drawn from an ensemble having entirely Gaussian joint PDFs) are fully described by second-order statistics. In the spatial domain second-order statistics are expressed by the autocovariance function C_0:

$$C_0(\mathbf{r}_1, \mathbf{r}_2) = \langle z(\mathbf{r}_1) z(\mathbf{r}_2) \rangle \in [-\sigma^2, \sigma^2] . \tag{4}$$

Equivalently, spatial second-order statistics can be expressed by the autocorrelation function C, which is

simply the autocovariance function normalized by the variance of $f_z(\zeta)$

$$C\left(\mathbf{r}_1, \mathbf{r}_2\right) = \frac{\langle z\left(\mathbf{r}_1\right) z\left(\mathbf{r}_2\right)\rangle}{\sigma^2} \in [-1, 1] . \tag{5}$$

For homogeneous, isotropic random processes $C\left(\mathbf{r}_1, \mathbf{r}_2\right)$ is a function only of the distance between the two points $C\left(R\right)$, where $R \equiv |\mathbf{r}_1 - \mathbf{r}_2|$ is termed the translation (sometimes termed the lag or slip). For such surfaces, a correlation length ℓ can be defined as the translation at which $C\left(R\right)$ first falls from its maximum $C\left(0\right) = 1$ to a specified value. Here, ℓ is defined as the translation for which $C\left(\ell\right) = 1/e$. In other words, the correlation length is a measure of the width of the central peak of the autocorrelation function. While a truly random process will have some value of translation for which $C\left(R\right)$ decreases to zero, $C\left(R\right)$ need not be a strictly decreasing function of translation. In fact, the surfaces of interest here are particularly distinguished by the existence of nonzero correlations for large values of translation (as discussed in Sec. II C).

The structure function (also termed the Allan deviation, the height-height correlation function, the mean-square increment function, or the variogram) is a spatial-domain second-order statistic equivalent to the autocorrelation function

$$S\left(R\right) = \left\langle \left[z\left(\mathbf{r}\right) - z\left(\mathbf{r} + R\right)\right]^2 \right\rangle , \tag{6}$$

and is related to the autocorrelation function by

$$S\left(R\right) = 2\sigma^2 \left[1 - C\left(R\right)\right] . \tag{7}$$

In the spectral domain, second-order statistics are given by the PSD. For homogeneous, one-dimensional random processes, the linear PSD $\mathfrak{p}\left(k_x\right)$ is related to the autocorrelation function and vice versa by a Fourier transform through the Wiener-Khintchine relation:

$$\mathfrak{p}\left(k_x\right) = \frac{\sigma^2}{2\pi} \int_{-\infty}^{\infty} C(R) e^{-\imath k_x R} dR , \tag{8a}$$

$$C(R) = \sigma^2 \int_{-\infty}^{\infty} \mathfrak{p}\left(k_x\right) e^{\imath k_x R} dk_x , \tag{8b}$$

where $k_x \in \left(-\infty, \infty\right)$ is the one-dimensional spatial wavenumber. When expressed in radial coordinates for isotropic two-dimensional random processes, the radial PSD $P\left(k\right)$ is related to the autocorrelation function and vice versa by a Hankel transform

$$P\left(k\right) = \frac{1}{2\pi} \int_0^{\infty} C\left(R\right) J_0\left(kR\right) R dR , \tag{9a}$$

$$C\left(R\right) = 2\pi \int_0^{\infty} P\left(k\right) J_0\left(kR\right) k dk , \tag{9b}$$

where J_0 is the zeroth-order Bessel function and $k \in \left(0, \infty\right)$ is the radial spatial wavenumber $k = \|\mathbf{k}\| = \sqrt{k_x^2 + k_y^2}$.

B. Power-Law Rough Surfaces

Spectral estimates made from measurements of sea-floor topography are often well modeled by PSDs that are inverse power-law functions of radial spatial wavenumber $P\left(k\right) \propto k^{-\gamma_2}$ with $\gamma_2 > 2$ [9, 10, 11, 12, 13, 14] and phase spectra that are uniformly distributed on $\left(0, 2\pi\right]$ [13, 14]. Because of the tractability of scattering

theories based on such spectra, characterizing sea-floor topography parametrically based on an inverse-power-law PSD is the dominant paradigm in underwater geoacoustics, among other areas of study.

A pure power-law PSD, for an isotropic surface, is given by

$$P(k) = \frac{w_2}{(h_0 k)^{\gamma_2}} \quad \text{for} \quad k \in (0, \infty) , \tag{10}$$

where h_0 is a reference length, usually taken to be unity, w_2 is the spectral strength in units of $(\text{length})^4$ (i.e., the value of the PSD at $k = h_0^{-1}$), and $\gamma_2 \in (2, \infty)$ is the two-dimensional spectral exponent.

In one dimension, (i.e., for a profile measured along a surface) the linear PSD is given by

$$\mathfrak{p}(k_x) = \frac{w_1}{(h_0 |k_x|)^{\gamma_1}} \quad \text{for} \quad k_x \in (-\infty, \infty) , \tag{11}$$

where $\gamma_1 = \gamma_2 - 1$, and

$$w_1 = \frac{\sqrt{\pi}}{h_0} \frac{\Gamma\left(\frac{1}{2}\gamma_1\right)}{\Gamma\left(\frac{1}{2}\gamma_2\right)} w_2 ,$$

as shown in Refs. 15 (pp. 12–15) and 2 (the Appendix A, pp. 2898–2899). (Note that both of the cited references contain typographical errors; the results reported here are correct.) Regardless of functional form, the radial PSD, $P(k)$, and linear PSD, $\mathfrak{p}(k_x)$, of an isotropic stochastic rough surface are related by the Abel transform [see Refs. 10 (the Appendix) and 15 (pp. 7–12)].

Note that $\mathfrak{p}(k_x)$ is truly a power-spectral *density* in that it has units $(\text{length})^3$, which are units of "power", $(\text{length})^2$, per elemental unit of wavenumber, $(\text{length})^{-1}$. Likewise, $P(k)$ has units $(\text{length})^4$, which are units of "power", $(\text{length})^2$, per elemental unit wavenumber, $(\text{length})^{-2}$. Consequently, for profiles,

$$\sigma^2 = \int_{-\infty}^{\infty} \mathfrak{p}(k_x) \, dk_x , \tag{12}$$

and, for surfaces,

$$\sigma^2 = \int_{-\infty}^{\infty} \mathfrak{p}(k_x) \, dk_x , \tag{13}$$

where σ^2 corresponds to the total "power" of $z(\mathbf{r})$.

General bounds on spectral exponent are expressed in terms of $\eth$, the topological dimension, by $\gamma_\eth \in (\eth, \infty)$, where $\eth = 1$ or 2. Topological dimension is related to d, the dimensionality of the embedding Euclidean space, by $d = \eth + 1$, such that the mapping describing the topography $\{z(\mathbf{r}) : \mathbf{r} \in \mathbb{R}^\eth\}$ corresponds to the graph of the mapping $\{(\mathbf{r}, z(\mathbf{r})) : \mathbf{r} \in \mathbb{R}^\eth\}$, which is in $\mathbb{R}^d$.

It is nonphysical for the PSD of surface topography to follow a power-law form for all k. The resulting surface has infinite RMS roughness because of the singularity of the PSD as $k \to 0$. Likewise, this nonphysical nature is reflected in the autocorrelation function [see Eq. (15) of Ref. 2], which results from the divergence of the integrals relating $C(R)$ to the PSD of power-law form. (However, the structure function [Eq.(6)] is defined for surfaces having a power-law PSD [16].) Physically realizable random rough surfaces must therefore have PSDs that depart from a simple power-law form for small k. A variety of PSDs for which power-law behavior has a low-frequency cutoff or is limited to finite bandwidth have been proposed; some of which are described below and plotted in Fig. 1. Particular attention has been given to PSDs for which $C(R)$, as given by Eqs.(8 and 9), can be given an analytical expression. This is of interest because it is $C(R)$ rather than $P(k)$ that enters directly into small-slope calculations of scattering from rough surfaces [2].

The simplest way to achieve a PSD having the needed small-k cutoff of power-law behavior is restricting the nonzero portions of a power-law PSD to bandwidth $[k_-, k_+]$ where $k_- > 0$ and k_+ may be infinite. The
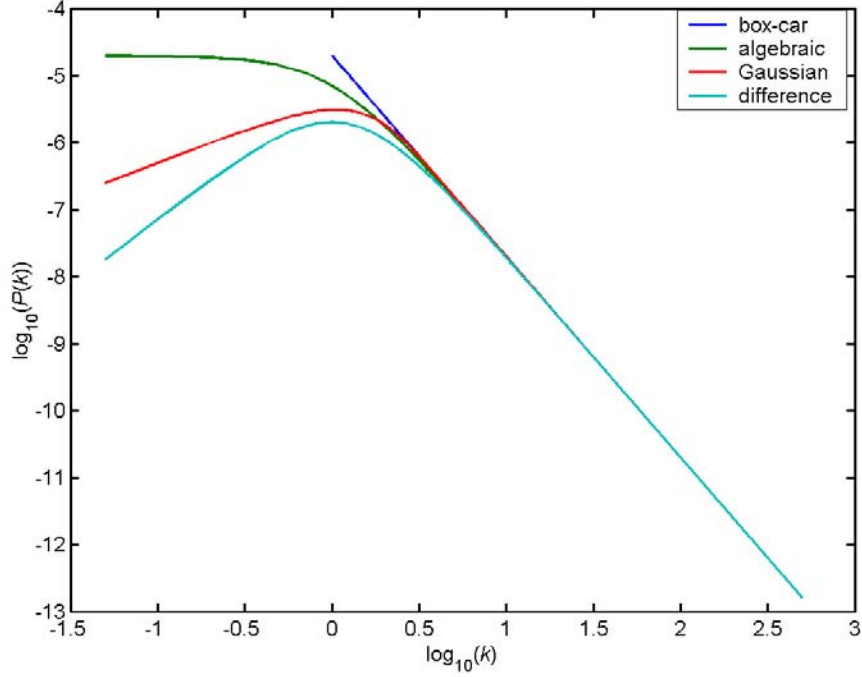
FIG. 1: Power-spectral density as a function of radial spatial wavenumber for each of the forms described in Sec. II B are compared for $\gamma_2 = 3.0$ and $w_2 = 2 \cdot 10^{-5}$ m^4. Small-k cutoff parameters have been adjusted to yield approximately equal cutoff points for each PSD.

resulting spectrum with 'box-car' cutoff is given by

$$P(k) = \begin{cases} \frac{w_2}{(h_0 k)^{\gamma_2}} & k_- \leqslant k \leqslant k_+ \\ 0 & \text{otherwise} \end{cases}, \tag{14}$$

and is depicted in Fig. 1. By forcing PSD to zero at $k = 0$, Eq.(14) assures that the resulting surface has no constant offset in height.

As an alternative to the abrupt transitions of the PSD proposed in Eq.(14), a form having finite power at small k, which may better represent PSD observed both in shallow-water (Ref. 17, p. 365) and deep-water ocean bottoms [10, 18], can be obtained from a power-law spectrum with an 'algebraic' cutoff at small k [2, 10]:

$$P(k) = \frac{w_2}{\left[(h_0 k)^2 + (h_0 k_L)^2 \right]^{\gamma_2/2}}, \tag{15}$$

as shown in Fig. 1. A power-spectral density of a similar form to Eq. 15 can be approximated by a piece-wise continuous function (not shown in Fig. 1) and generalized to include a large-wavenumber cutoff [19], which is helpful for modeling real PSDs measured on a regular array of points (see Sec. III A 1):

$$P(k) = \begin{cases} \frac{w_2}{h_0 k_L^{\gamma_2}} & k < k_L \\ \frac{w_2}{h_0 k^{\gamma_2}} & k_L \leqslant k \leqslant k_H \\ 0 & k > k_H \end{cases}. \tag{16}$$

Surfaces described by Eqs.(15 and 16) have nonzero mean height, which can be removed by detrending as

6

described in Sec. III C 1.

Observed PSDs sometimes display positive slope (power decreasing with wavenumber) below a cutoff frequency, which may be an artifact of detrending the measured profiles [20]. Power-spectral density of this form, shown in Fig. 1, can be realized by a power-law spectrum with a 'Gaussian' cutoff at small k, which results from subtracting the Gaussian-weighted moving average of the topography from a surface having power-law PSD, as described in Ref. 21:

$$P(k) = \frac{w_2}{(h_0 k)^{\gamma_2}} \left\{ 1 - \exp\left[-(ka_L)^2 \Big/ 2 \right] \right\}^2 . \tag{17}$$

However, $C(R)$ corresponding to this PSD is not analytically expressible.

A similar low-frequency cutoff, but with $C(R)$ that is analytically expressible, is achieved by a PSD written as the difference between two power-law PSDs having algebraic small-k cutoffs [22, 23].

$$P(k) = P_1(k) - P_2(k) , \tag{18a}$$

$$P_1(k) = \frac{b_1}{\left[1 + (b_2 h_0 k)^2 \right]^{\gamma_2/2}} , \tag{18b}$$

$$P_2(k) = \frac{b_1}{\left[1 + \left(\frac{b_2 h_0 k}{a_2} \right)^2 \right]^{\gamma_2/2}} , \tag{18c}$$

as shown in Fig. 1. The spectral strength w_2 and the location of the spectral peak k_p are related to the parameters of the difference spectrum a_2, b_1, and b_2 through

$$b_1 = \frac{w_2 b_2^{\gamma_2}}{1 - a_2^{\gamma_2}} , \tag{19a}$$

$$b_2 = \frac{1}{h_0 k_p} \left(\frac{a_2^{\frac{2}{1+\gamma_2/2}} - 1}{1 - a_2^{\frac{2}{1+\gamma_2/2} - 2}} \right)^{\frac{1}{2}} , \tag{19b}$$

where a_2 determines the steepness of $P(k)$ about $k = k_p$.

While spectral exponent γ_2 is often assumed constant throughout the region of support of $P(k)$, it has been found that γ_2 of real surfaces sometimes varies with k [24, 25, 26]. Herzfeld $et\ al.$ have observed that spectral exponent is greater at large k than at small k for measurements of deep-water ocean bottoms made over length scales 5 m–80 km and 1 m–600 km (see Ref. 25 and Refs. therein). At much smaller scales, 0.05 mm–3.5 m, Briggs $et\ al.$ have found similar results for measurements of shallow-water granular ocean bottoms. This increase in spectral slope at large k is often associated with grain size of the constituent materials [24, 27]. Measured values of w_2 and γ_2 for real ocean bottoms are described in Sec. II E.

C.   Fractal Rough Surfaces

That real topography is taken to be the realization of a random process having $P(k) \propto k^{-\gamma_2}$ has significant implications for how it is characterized. Power spectra of this form are frequently encountered in time-series analysis, where random sequences $z(x)$, $(\mathfrak{d} = 1)$, having spectra $\mathfrak{p}(k_x) \propto k_x^{-\gamma_1}$, $\gamma_1 \in (0, \infty)$ are termed $1/f^\alpha$ or 'fractional' noise.

The range of random sequences of this form is bound by Gaussian white noise, having $\gamma_1 = 0$, and

Brownian motion (realizations of the Wiener process, sometimes termed Brown noise), having $\gamma_1 = 2$. These two bounding sequences are related in that Gaussian white noise is (formally, over smoothed intervals) the derivative (or 'increments process') of Brownian motion.

Brownian motion (and consequently Gaussian white noise) can be defined axiomatically [6, 28].

Theorem 1. *The process $\{z\}$ is a continuous Brownian motion if $\forall\ \Delta x$ the increments $\Delta z(x) = z(x + \Delta x) - z(x)$ satisfy*

1. *Gaussian distribution*

2. *zero mean*

3. *variance $\propto \Delta x$*

4. *successive increments $\Delta z(x)$ and $\Delta z(x + \Delta x)$ are uncorrelated .[84]*

An axiomatic definition for all $1/f^\alpha$ noise is arrived at by generalizing the axiomatic definition of Brownian motion [29].

Theorem 2. *The process $\{z\}$ is a continuous fractional Brownian motion (FBM) if $\forall\ \Delta x$ the increments $\Delta z(x) = z(x + \Delta x) - z(x)$ satisfy*

1. *Gaussian distribution*

2. *zero mean*

3. *variance $\propto \Delta x^{2\mathfrak{H}}$, where $\mathfrak{H} \in (0, 1]$ is the Hurst exponent*

4. *successive increments $\Delta z(x)$ and $\Delta z(x + \Delta x)$ are correlated with correlation coefficient given by $2^{2\mathfrak{H}} = 2 + 2\xi$ where $\xi \in \left(-\frac{1}{2}, 1\right)$.*

Such random processes are termed *fractional* Brownian motion (FBM) because of their noninteger spectral exponents. The spectral exponent γ_1 of FBM can be expressed in terms of the Hurst exponent by $\gamma_1 = 2\mathfrak{H} + 1$ (Ref. 30, p. 67). The derivative (increments process) of FBM is termed fractional Gaussian noise (FGN). Together FBM and FGN span an important segement of all $1/f^\alpha$ noise, with FBM having $\gamma_1 \in (1, 3]$ and FGN having $\gamma_1 \in [-1, 1]$. The only Gaussian process that is both self-affine and has stationary increments is FBM [31]. Fractional Brownian motion (though not FGN) can be generalized from random sequences ($\mathfrak{d} = 1$) to random fields ($\mathfrak{d} = 2$) and, thus, can serve as a model for the topography of random rough surfaces having a power-law PSD.

It is particularly notable that FBM lacks an inherent length scale. Stochastic processes that have this property are termed self-affine and are characterized by their Hurst exponent $\mathfrak{H} \in (0, 1]$. A real-valued stochastic process is self affine with Hurst exponent $\mathfrak{H}$ if its increments process $\Delta z(\vartheta) = z(\mathbf{r} + \vartheta) - z(\mathbf{r})$ satisfies the homogeneity relation

$$\{\Delta z(\lambda\vartheta)\} \doteq \{\lambda^{\mathfrak{H}}\Delta z(\vartheta)\} \ \forall\ \lambda, \mathbf{r}, \text{and } \vartheta\ , \tag{20}$$

where λ is a constant scale factor, and $\doteq$ denotes statistical equality, or, more exactly, equality of the finite-dimensional distributions [32, 33]. This homogeneity relation implies that empirical histograms of increments processes should be nearly equal when scaled according to Eq. 20. Because Eq. 20 is valid for all ϑ, the homogeneity relation also holds for the process itself [31]

$$\{z(\lambda\mathbf{r})\} \doteq \{\lambda^{\mathfrak{H}}z(\mathbf{r})\} \ \forall\ \lambda\ . \tag{21}$$

Consequently, self-affine surfaces are (statistically) invariant under transformations of the form

$$(x, y, z) \Rightarrow \left(\lambda x, \lambda y, \lambda^{\mathfrak{H}} z \right) \ . \tag{22}$$

If $\mathfrak{H} = 1$, FBM is self-similar and appears (statistically) identical when observed at all length scales. This is impossible for single-valued topography that can be expressed by the mapping described in Sec. II A, for which smaller features implictly have steeper slope than larger features [34, 35]. If $\mathfrak{H} < 1$, FBM appears (statistically) identical (e.g. self-similar) only if the z-axis is scaled independently of the other axes.

A property of self-affinity is dependence of surface measures (or, more exactly, the expectation values of these measures for the process) on observation length, i.e. FBM is nonstationary. For example, the RMS roughness [32, 33] and the structure function obey scaling relationships

$$\sigma \left(L \right) \doteq \sigma \left(L_0 \right) \left(\frac{L}{L_0} \right)^{\mathfrak{H}} \ , \tag{23a}$$

$$S \left(L \right) \doteq S \left(L_0 \right) \left(\frac{L}{L_0} \right)^{\mathfrak{H}} \ , \tag{23b}$$

where L is the length of an interval $[0, L]$ contained in the total interval $[0, L_0]$ of length L_0. Only in the case that $\mathfrak{H} \to 0$ are surface measures independent of profile length and is FBM a stationary random process.

In the case of FBM, $\mathfrak{H}$ can be thought of as a parameter that determines the "rate at which roughness changes scale," [36] such that smaller values of $\mathfrak{H}$ correspond to larger variations in small-scale topography. This behavior can be categorized via the concept of 'persistence', which describes the extent to which consecutive elements of increments process of $z \left(r \right)$ are correlated. Realizations of FBM with $\mathfrak{d} = 1$ have $\mathfrak{H} \in (0, 1)$. For $\mathfrak{H} \in (0, 1/2)$ FBM is antipersistent, with negative correlation between consecutive increments and noise-like spatial variation. For $\mathfrak{H} \in (1/2, 1)$ FBM is persistent with positive correlation between consecutive increments and more regular spatial variation. In the case that $\mathfrak{H} = 1/2$, FBM reduces to conventional (or 'chaotic') Brownian motion with uncorrelated increments.

The graphs of realizations of FBM are one of a class of geometries termed fractals—a term first coined by Mandelbrot [28] to describe profiles and surfaces that display complexity not well described by their topological or Euclidean dimensionality. Fractals can be formally (but not inclusively) defined as sets for which the Hausdorff-Besicovitch dimension H exceeds the topological dimension $\mathfrak{d}$ (Ref. 6, p. 15). Fractals may be either deterministic or stochastic. When encountered in nature, fractals are almost exclusively stochastic. In other words, they are realizations of random processes, like FBM.

The Hausdorff-Besicovitch dimension, $H \in [\mathfrak{d}, d)$, is a measure of the space-filling quality of a fractal object. A smooth profile ($\mathfrak{d} = 1$, d=2) has $H = 1$ and a smooth plane ($\mathfrak{d} = 2$, d=3) has $H = 2$. While computing H of a set is complicated (Ref. 6, pp.362–365,458–459), H of self-affine profiles and surfaces is equivalent to more simply computed dimensions, such as the box dimension [37]. For $\mathfrak{d} = 1$, the box dimension B is given by

$$B = \lim_{\chi \to 0^+} \frac{- \log n}{\log \chi} \ , \tag{24}$$

where n is the number of boxes of linear size χ needed to cover the set of points $\mathcal{S} \in \mathbb{R}$ defining the profile.

The Hausdorff-Besicovitch dimension is essentially a local property of a profile or surface [Refs. 6 (p. 373) and 38]. In contrast, the Hurst exponent characterizes long-range correlation on a global scale. While not true for all fractals [38], for self-affine fractals, such as FBM, the two aspects are interrelated. For self-affine random fractals, the Hurst exponent (global property) is related to the Hausdorff-Besicovitch

dimension (local property) by [see Refs. 39 (pp. 301–325) and 6 (p. 373)]

$$H = d - \mathfrak{H} \tag{25}$$

such that smaller $\mathfrak{H}$ corresponds to larger H and a rougher surface.

Topothesy (or 'crossover length') τ is a measure of the 'strength' of a fractal and is defined as the horizontal distance (i.e., R) between two points connected by a line of RMS slope one radian [11, 16, 40]. For an isotropic rough surface, τ is identical for the surface ($\mathfrak{d} = 2$) and profiles formed by cutting the surface ($\mathfrak{d} = 1$). Topothesy can be alternatively defined in terms of the structure function

$$S(\tau) = \tau^2 \; \forall \; \mathfrak{d} \; . \tag{26}$$

The RMS roughness measured over a profile of length L, $\sigma(L)$, is related to topothesy through the scaling argument

$$\sigma(L) = \tau^{1-\mathfrak{H}} L^{\mathfrak{H}} \; , \tag{27}$$

where $\sigma(\tau) = \tau$.

Together the Hausdorff-Besicovitch dimension (or, alternatively, the Hurst exponent) and topothesy provide a complete description of an isotropic, self-affine stochastic fractal surface.

1. Spectra of fractals

As conjectured by Mandelbrot and Van Ness (Ref. 29, p. 436) and later shown by Flandrin [41, 42], the formally averaged PSD of FBM is given by the power-law $P(k) \propto k^{-2\mathfrak{H}-1}$.

The Hausdorff-Besicovitch dimension of FBM (of arbitrary $\mathfrak{d}$) is given by [16, 43]

$$H = 1 + \mathfrak{d} + (\mathfrak{d} - \gamma_{\mathfrak{d}})/2 \qquad \text{for} \quad \gamma_{\mathfrak{d}} \in (\mathfrak{d}, \mathfrak{d}+2] \tag{28}$$

Because Eq. (28) breaks down for $\gamma_{\mathfrak{d}} > \mathfrak{d} + 2$, it is often argued that $\gamma_2 \in (\mathfrak{d}, \mathfrak{d}+2)$. However, $\gamma_{\mathfrak{d}} > \mathfrak{d} + 2$ simply corresponds to nonfractal differentiable profiles or surfaces of $H = \mathfrak{d}$ having smoothness increasing with $\gamma_{\mathfrak{d}}$ [24, 44]. Such a conclusion is further confirmed by experimental measurements of spectral exponents that are larger than the proposed limits (see, e.g., Ref. 12).

Profiles and surfaces can be categorized based on fractal dimension, as determined by spectral exponent. For profiles ($\mathfrak{d} = 1$), $\gamma_1 \in (1,3] \Rightarrow H \in (2,1]$:

- $\gamma_1 = 1$, $H = 2$: extreme fractal (borderline area filling)

- $\gamma_1 = 2$, $H = 1.5$: Brownian fractal (graph of one-dimensional Wiener process)

- $\gamma_1 = 3$, $H = 1$: marginal fractal (borderline nonfractal) .

Five profiles that are realizations of FBM are shown in Fig. 2. Fractal dimensions of these profiles range from 2 to 1 in uniform increments of 0.25.

For surfaces ($\mathfrak{d} = 2$), $\gamma_2 \in (2,4] \Rightarrow H \in (3,2]$:

- $\gamma_2 = 2$, $H = 3$: extreme fractal (borderline volume filling)

- $\gamma_2 = 3$, $H = 2.5$: Brownian fractal (graph of two-dimensional Wiener process)

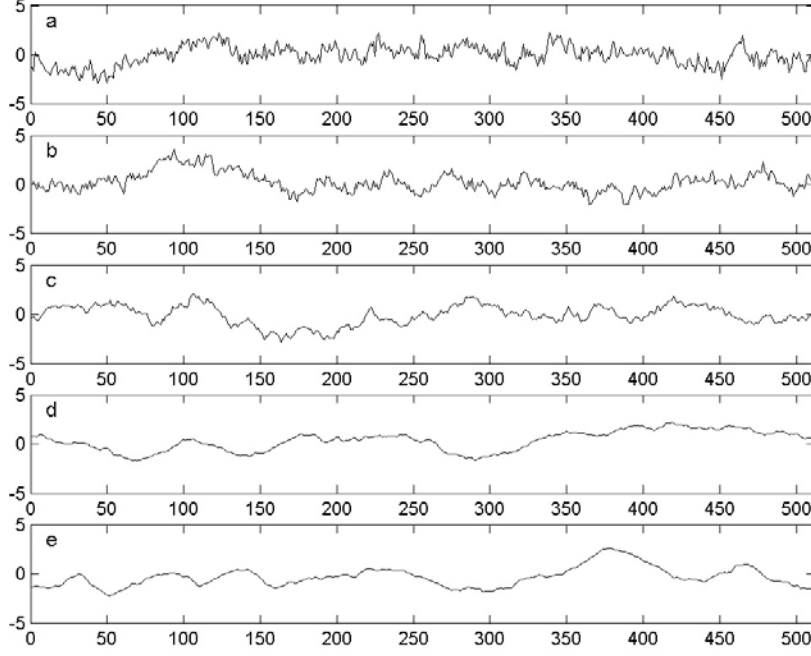- $\gamma_2 = 4$, $H = 2$: marginal fractal (borderline nonfractal) .

FIG. 2: Realizations of FBM for the range of Hausdorff-Besicovitch dimension $H \in [2, 1]$. Hausdorff-Besicovitch dimensions are 2 (a), 1.75 (b), 1.5 (c), 1.25 (d), 1 (e). The y-axis is in normalized units,as the amplitudes of the zero-mean profiles are normalized by σ. The x-axis is in arbitrary units (sample number)

The topothesy of a FBM profile ($\mathfrak{d} = 1$) or surface ($\mathfrak{d} = 2$) is related to power-law parameters by [45]

$$\tau^\alpha = \frac{w_2 \pi^{\mathfrak{d}/2} 2^\alpha \Gamma(\alpha/2)}{h_0 (\gamma_{\mathfrak{d}} - \mathfrak{d}) \Gamma(\gamma_{\mathfrak{d}}/2)} \qquad \text{for} \quad \gamma_{\mathfrak{d}} \in (\mathfrak{d}, \mathfrak{d} + 2) \ , \tag{29}$$

where $\alpha = \mathfrak{d} + 2 - \gamma_{\mathfrak{d}}$ such that, for isotropic surfaces ($\mathfrak{d} = 2$),

$$w_2 = \frac{\pi (\gamma_2 - 2) \Gamma\left(\frac{\gamma_2}{2}\right)}{2^{2-\gamma_2} \Gamma\left(\frac{4-\gamma_2}{2}\right)} \tau^{4-\gamma_2} \frac{2}{(2\pi)^{\gamma_2}} \ . \tag{30}$$

2. Band-limited fractals

The power-law PSD of self-affine stochastic fractal profiles and surfaces, such as FBM, is problematic when the power-law functional form is assumed to exist for all k, as discussed in Sec. II B. FBM cannot be easily characterized using conventional metrics, such as those described in Sec. II A. In particular, realizations of FBM possess mulitscale roughness such that they are continuous but nondifferentiable. Additionally, they display long-range correlations over a range of translations limited only by the physical extent of the particular realization. Self-affinity violates assumptions of (wide-sense) stationarity due to dependence of measured quantities (e.g., σ) on sample size, while long-range correlations violate assumptions of ergodicity due to the inability of any finite spatial-averaging domain to be large enough to recover all information about the random process [46].

Real surfaces can be self-affine only over a "finite hierarchy of scales" [45]. Such surfaces can be said

11

to be "approximately self-affine" [45] or to posses "limited self-affinity" [47]. At large scales, the finite extent provides a small-k limit. At small scales, the molecular or granular structure provides a large-k limit. Alternatively, small-scale limits of self-affinity can result from the limited resolution of manufacturing processes, in the case of fabricated rough surfaces, or as an artifact of finite-resolution measurement methods, when data from from real surfaces are analyzed.

Rough surfaces are therefore better modeled as *approximately* self-affine, having band-limited PSDs, such as those given in Sec. II B. Doing so has a number of advantages. In particular, conventional metrics, such as RMS roughness, σ, and autocorrelation, $C(R)$, which are not well defined for FBM, can be defined unambiguously for band-limited FBM. It has been shown that both FBM profiles [41] and surfaces [48] having power-law PSD restricted to a finite band (with some additional conditions on the falloff outside of the band) are wide-sense stationary. Likewise, band-limited FBM profiles and surfaces are differentiable, due to the large-k cutoff.

However, limiting the hierarchy of scales of self-affinity for a self-affine fractal can alter the Hausdorff-Besicovitch dimension H from that of the equivalent, ideally self-affine fractal [49, 50, 51, 52, 53]. The relationship between H and γ_0 given in Eq. (28) holds only for ideally self-affine fractals. Band limiting in the spatial-wavenumber domain alters the form of the structure function, $S(R)$, such that the linear relationship between $\log S(R)$ and $\log R$ extends only over the scaling interval $R \in (R_-, R_+)$, defined by [50]:

$$R_- = \left[\frac{\sqrt{\pi}}{\gamma_1 - 1} \frac{\Gamma(H)}{\Gamma(\gamma_1/2)} \right]^{1/(3-\gamma_1)} \frac{2}{k_{x,-}} , \tag{31a}$$

$$R_+ = \left[\frac{\Gamma(\gamma_1/2)}{\sqrt{\pi}\Gamma(H-1)} \right]^{1/(\gamma_1-1)} \frac{2}{k_{x,+}} , \tag{31b}$$

where H is the Hausdorff-Besicovitch dimension of an ideal self-affine fractal having the same spectral exponent ($H = (5 - \gamma_1)/2$).

Similarly, topothesy, as defined by Eq. (26), is a function of the shape and location of small- and large-k cutoffs, which alter the form of the structure function [19]. The small-k cutoff is manifest as oscillations in $S(R)$ (or, alternatively, $C(R)$) at large R [7, 50]. The large-k cutoff is also manifest as oscillations, which are noticeable only for large σ [50].

An alternative definition of τ, based on an analytic expression for $S(R)$, is independent of wavenumber cutoffs. The band limited power-law PSD given by Eq. (14) has $S(R)$ that is expressible as an asymptotic expansion [50, 54] the first term of which is $S(R)$ of an ideally self-affine fractal

$$S(R) = \tau^{\partial+2-\gamma_0} R^{\gamma_0-\partial} . \tag{32}$$

Defining τ by the above expression leads to a form that is independent of the spectral cutoffs.

D. Parameter Study: Realizations of Band-Limited Fractal Surfaces

This section presents a series of realizations of a band-limited FBM surface. These are shown in Figs. 3–6 and described in Table I. These figures are grouped into two series, as indicated in Table I: Fig. 3 is a movie (with frames shown individually in the Appendix as Figs. 13–18) illustrating the the effect of increasing γ_2; Figs. 4–6 show the dependence on low-wavenumber cutoff [here ka_L of Eq. (17)].

Varying γ_2 and ka_L produces changes in the realized surface that can be appreciated visually (the parameter w_2 simply acts as a scale factor). In the movie shown in Fig. 3 (and also Figs. 13–18 of the Appendix), γ_2 is varied for a particular realization while the other two parameters are fixed. Varying γ_2

12

TABLE I: Realizations of a band-limited fractal surface. All cases have $h_0 = 1$m and $w_2 = 10^{-5}$ m^4.

γ_2	2.0	2.4	2.8	3.2	3.6	4.0	2.8	2.8	2.8
ka_L	0.05	0.05	0.05	0.05	0.05	0.05	0.01	0.05	0.10
Figure	13^a	14^a	15^a	16^a	17^a	18^a	4	5	6

[a]Collected in Fig. 3 as one frame of an embedded QuickTime animation.

introduces a change in the overall length scale, but as the idealized distribution of heights is Gaussian, the range of heights can be approximately standardized by subtracting the mean height of the entire realization and dividing by the standard deviation of the heights. In each figure (including the figures in the appendix), the x and y axes are in units of meters and the z-axis (represented by the color bar) is in normalized units arrived at by dividing by σ. As such, realizations are presented using the same color scale. It is observed that the graininess of various features decreases as γ_2 increases, until the surface looks qualitatively different from the $\gamma_2 = 2$ surface. This is related to the behavior of the correlation function, as the values at small lags can differ considerably for smaller values of γ_2.

The particular plotting technique chosen results in certain features of the surface being perceived as islands, the boundaries of which have a level of detail that varies with the fractal dimension of the surface. In this way, the presentation is similar to the "zero set" of the elevation data formed by the intersection of the surface with a plane oriented parallel to the nominal surface orientation. The fractal dimension of the boundaries of the islands formed is thus one less than the fractal dimension of the surface itself. [55]

Figures 4–6 show the results of varying the low-k cutoff. In comparison with Fig. 5, which has the same value of $\gamma_2 = 2.8$ as Figures 4 and 6, there is an observable qualitative effect that changing the cutoff produces a change in the apparent values of γ_2, the high cutoff value producing a realization that has an apparent γ_2 greater than 3.

E.   Rough Surface Experiments with Physical Models

As stated in the Introduction, rough-surface experiments with physical models become highly useful when a systematic field experiment is impractical, as in a controlled experiment with bottom roughness parameters. While it is difficult to create physical models that are exact acoustic analogs of real ocean bottoms over a complete set of parameters (such as density, shear/compressional speed, and shear/compressional attenuation), a physical model can be constructed to exhibit scattering behavior analogous to a real ocean bottom, such as a strong dependence on a particular parameter.

As an example, Carolina Coast limestone is a type of elastic ocean bottom for which the scattering behavior has a large predicted dependence on γ_2. At two sites off the Carolina Coast, Soukup and Gragg [56] extracted values of w_2 and γ_2 using a geoacoustic inversion technique that analyzed scattering-strength vs. grazing-angle curves in the band 2–3.5 kHz in water depths of 230–310 m under the assumption that interface scattering wholly dominated any volume-scattering effects. The inverted spectral parameters for the Carolina Coast limestone obtained by Soukup and Gragg [56] were $\gamma_2 = 2.6 - 2.8$ and $w_2 = 4 \cdot 10^{-4} - 9 \cdot 10^{-4}$. The scattering strength for this limestone predicted by the NRL small-slope model [2] is plotted in Fig. 7 as a function of grazing angle for different values of γ_2 at 3500 Hz.

Limestone supports both compressional and shear waves, each with associated critical angles. Particularly characteristic of the behavior of limestone is a clear stratification of scattering strength as a function of γ_2 below the lowest (shear-speed) critical angle. To investigate this substantial dependence of scattering strength on γ_2, the predicted behavior of PVC, a material with analogous backscattering behavior,
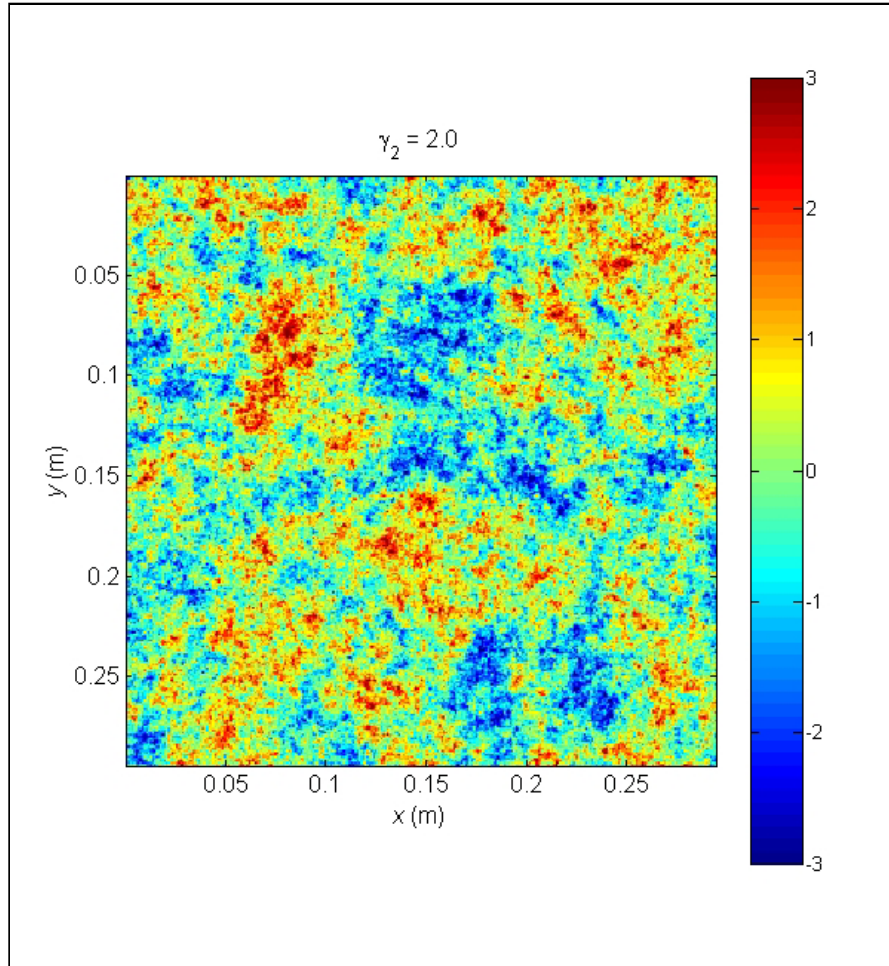
13

FIG. 3: Embedded QuickTime animation illustrating the changes observed in realizations of band-limited fractal surfaces with as γ_2 varies from 2 to 4, for fixed $w_2 = 1 \cdot 10^{-5} \, \text{m}^4$ and $ka_L = 0.05$. (See Table I.)

was studied. Below the compressional-speed (p-wave) critical angle for PVC at 300 kHz, the dependence of scattering strength on γ_2 is even more pronounced than for limestone. (Though PVC supports shear waves, the speed of these waves is such that no shear-wave critical angle exists.) An example is shown in Fig. 8. Scattering strengths from a rough PVC sheet at the Allied Geophysical Laboratory/University of Houston were obtained and the mean behavior of the scattering was comparable to the predictions of the NRL small-slope scattering model [57]. The PVC sheet had mean values of w_2 and γ_2 of $1.5 \cdot 10^{-5} \, \text{m}^4$ and 2.9, respectively. The authors are currently fabricating rough surfaces from PVC that will represent other values of w_2 and γ_2. Future research will also introduce different materials so that other predicted effects of the small-slope theory, such as local minima at particular grazing angles, can be verified. While the lowest-order small-slope predictions shown here were the motivation for the authors' experimental design, modeling the actual scattering behavior for such surfaces may require the use of a higher-order model for surface scattering and a model of scattering in the subsurface volume.

III.   FABRICATION OF ROUGH SURFACES

Creating a physical realization of a random rough surface is a two-step process. The first of these steps is the numerical generation of the topography. Section III A describes how this can be achieved by a spectral
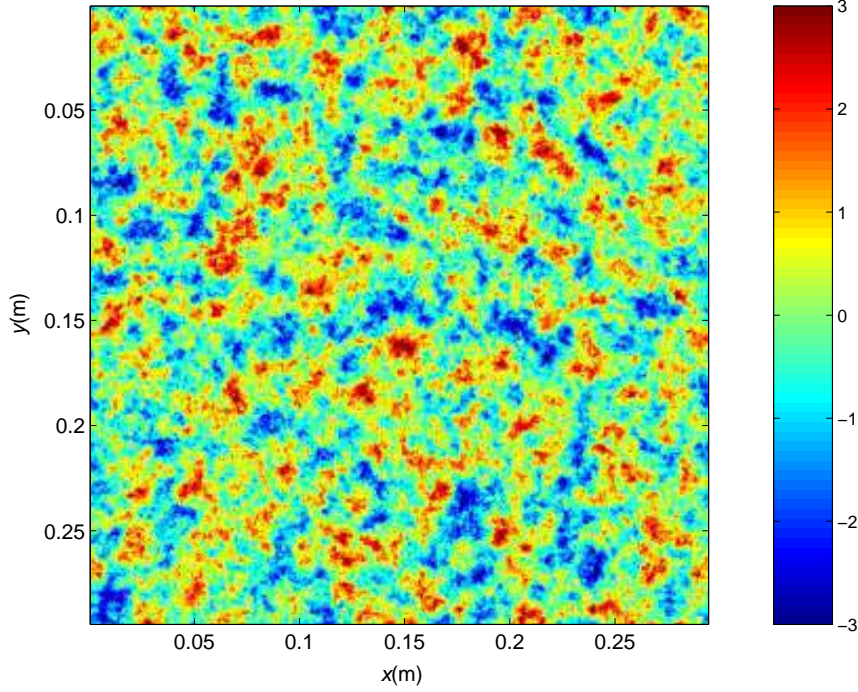
14

FIG. 4: Realization of a band-limited fractal surface with $w_2 = 1 \cdot 10^{-5}\ \text{m}^4$, $\gamma_2 = 2.8$, and $ka_L = 0.01$. (See Table I.)

method. In this section the theoretical effects of the finite size of the realization and the requirement that the surface be defined only over a discrete grid of points are also considered. The second step of creating a physical realization of a random rough surface is physically manufacturing the generated topography. Section III B describes how this can be achieved using a computer-numerically controlled milling machine. In practice, the topography of a physically manufactured surface must be measured to inspect for accuracy of the manufacturing process. Such a measurement process, using a touch-trigger probe, is described in Sec. III C.

A. Generating Surface Realizations

When modeled as a random field, the topography of a particular rough surface $z(\mathbf{r})$ is a realization of a particular two-dimensional random process. Taking FBM as a model of random rough surface topography, the first step in fabricating a rough surface is generation of a realization of FBM.

The earliest methods for generating realizations of FBM utilized the Weierstrass-Mandelbrot function [58]. This extension of the Weierstrass function [59, 60], first proposed by Mandelbrot [28], represents profiles $(\mathfrak{d} = 1)$ by

$$\Re\left[W(x)\right] = \sum_{n=-\infty}^{\infty} \frac{\left[\left(1 - e^{i\alpha^n x}\right) e^{i\phi_n}\right]}{\alpha^{(2-H)n}}\ , \tag{33}$$
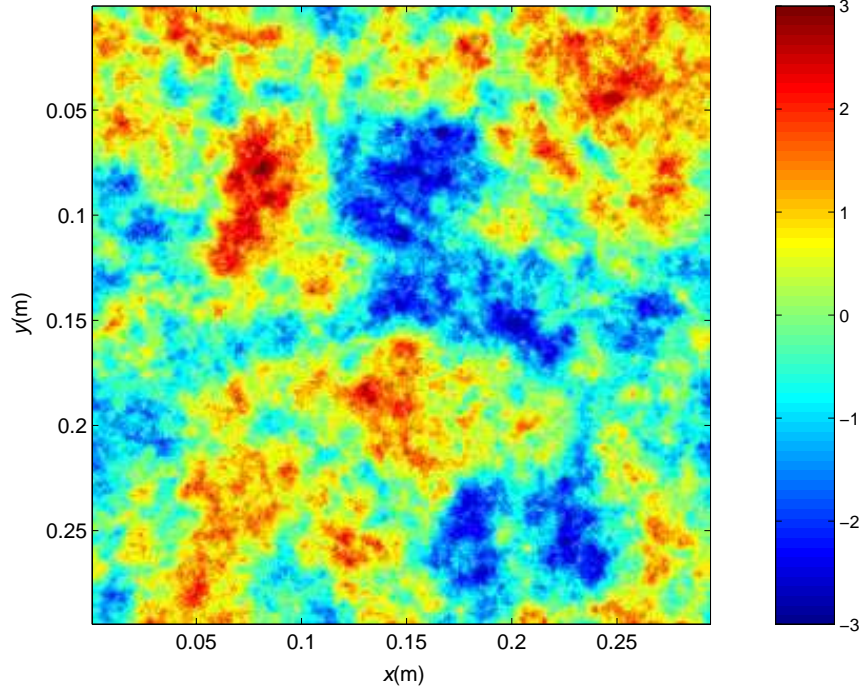
15

FIG. 5: Realization of a band-limited fractal surface with $w_2 = 1 \cdot 10^{-5} \, \text{m}^4$, $\gamma_2 = 2.8$, and $ka_L = 0.05$. (See Table I.)

where $\alpha > 1$ is a parameter and ϕ_n is the phase, a random variable uniformly distributed on $(0, 2\pi]$. Equation (33) describes a summation of sinusoids having the geometric spectrum of wavenumbers $k_x = \alpha^n$, the so-called Weierstrass spectrum, and amplitudes $\propto k_x = \alpha^n$. The Weierstrass-Mandelbrot function is known to be a fractal [28, 58, 61] and has a mean PSD consistent with FBM [58].

While first used only to describe fractals generated by Eq.(33), as in Ref. 58, the term Weierstrass-Mandelbrot fractal has been informally extended to describe similar summations of sinusoids having different wavenumber spectra. In particular, those defined on spectra of algebraic intervals, such as the Fourier spectrum [47], can also be termed Weierstrass-Mandelbrot fractals. Berry and Lewis [58] were first to use the Weierstrass-Mandelbrot function, defined over the Weierstrass spectrum, as models of FBM ($\mathfrak{d} = 1$). Equivalent synthesis over the Fourier spectrum is discussed in Ref. 62 (pp. 76–77). Kumar and Bodvarsson [63] later extended these methods to surfaces ($\mathfrak{d} = 2$), both for Weierstrass and Fourier spectra. (See also Ref. 62, pp. 174–187.)

When defined over the Fourier spectrum, the Weierstrass-Mandelbrot function is essentially equivalent to an inverse Fourier transform of a k-space (spatial-wavenumber domain) description of FBM consisting of a power-law PSD and a random phase spectrum. Here the Fourier method is chosen for the numerical generation of surface realizations because discrete Fourier transforms on finite, uniform grids can be efficiently calculated by the fast Fourier transform (FFT).
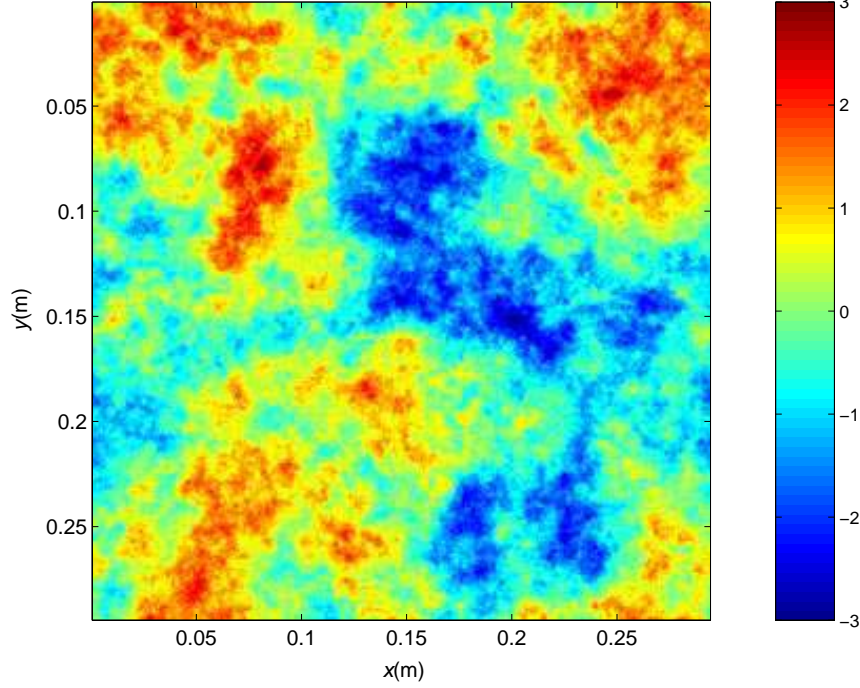
16

FIG. 6: Realization of a band-limited fractal surface with $w_2 = 1 \cdot 10^{-5} \text{ m}^4$, $\gamma_2 = 2.8$, and $ka_L = 0.1$. (See Table I.)

1. Spatial sampling and surfaces of finite extent

For the numerical generation of surface realizations, $z(\mathbf{r})$ is expressed by a finite two-dimensional array representing surface heights sampled on a uniform grid. The relation between the spatial-sampling interval Δx and the maximum resolvable linear spatial wavenumber $\hat{k}_x = \max(|k_x|)$ in each Euclidean dimension (equivalent to the Nyquist frequency), is given by the Whittaker-Shannon-Kotel'nikov (WSK) sampling theorem [64]

$$\hat{k}_x = \pi/\Delta x \ . \tag{34}$$

For isotropic surfaces sampled on a uniform grid ($\Delta x = \Delta y$), the maximum radial spatial wavenumber is $\hat{k} = \sqrt{2}\hat{k}_x$.

The relation between the linear extent of the surface (region of support) X and the minimum resolvable linear spatial wavenumber $\check{k}_x = \min(|k_x|)$ in each Euclidean dimension (that for which one wavelength corresponds exactly to the linear extent of the surface) is

$$\check{k}_x = 2\pi/X \ . \tag{35}$$

Clearly, $k_x < \check{k}_x$ can influence the piston (zeroth-order polynomial term), tilt (first-order polynomial term), and curvature (second- and higher-order polynomial terms) of the surface, though detrending strongly
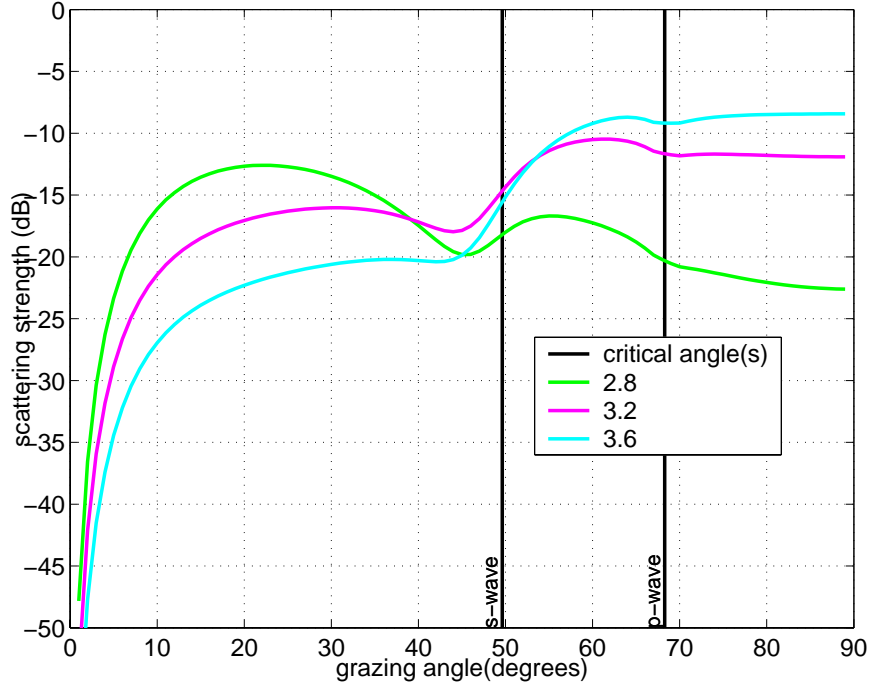
17

FIG. 7: Lowest-order small-slope model predictions of the backscattering strength *vs.* grazing angle at three values of γ_2 for an incident wave of 3 kHz scattered from a limestone bottom of the Carolina Coast, with a w_2 value, density, shear/compressional speeds, and shear/compressional attenuations inverted from at-sea experimental data [56]. Note the stratification of scattering levels as a function of γ_2 predicted for angles below the shear-speed (*s*-wave) critical angle.
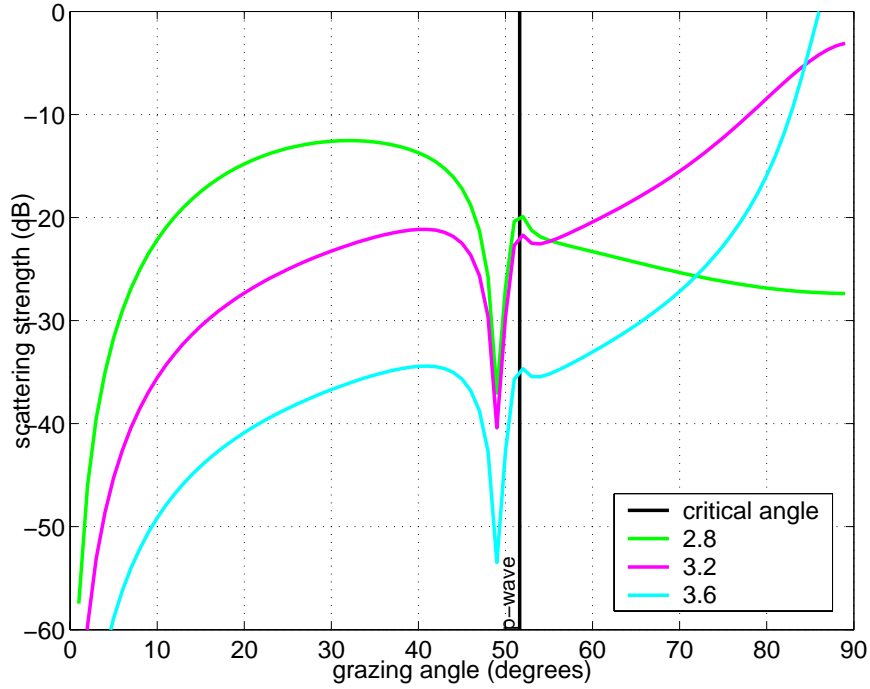
FIG. 8: Lowest-order small-slope model predictions of the backscattering strength *vs.* grazing angle at three values of γ_2 for an incident wave of 300 kHz scattered from the Houston PVC sheet, with a w_2 value obtained from profilometry and the density, shear/compressional speeds, and shear/compressional attenuation measured from a sample of the material. Note the wide (in comparison with Fig. 7) disparity in the scattering levels for angles below the compressional-speed (*p*-wave) critical angle. Verifying this disparity is one goal of the tank experiments currently underway at NRL.

18

suppresses $k_x < \check{k}_x$ [20]. For surfaces realized on a square surface of support $(X = Y)$, the minimum radial spatial wavenumber is $\check{k} = \sqrt{2}\check{k}_x$. The observed PSD of a physically realized power-law surface can be modeled by Eq. (14) where $k_L = \check{k}$ and $k_H = \hat{k}$.

2. Fractal properties

Discrete, finite-support realizations of FBM are approximately self-affine, band-limited fractals. The length-scale range x_- to x_+ over which a such a profile or surface is self-affine is determined by (1) the spatial sampling interval Δx, which sets the large-k limit x_- and (2) the extent of the region of support X, which sets the small-k limit x_+. Specifically,

$$x_- = \frac{\Delta x}{2} \,, \tag{36a}$$

$$x_+ = \frac{X}{2} \,. \tag{36b}$$

3. Computational procedure

In this work, approximately self-affine, band-limited realizations of FBM are generated by a spectral method in which a representation of the surface $Z(\mathbf{k})$ is created in k-space (the spatial-wavenumber domain) and then transformed into a representation $z(\mathbf{r})$ in real space (the spatial domain) using the discrete Fourier transform (DFT).

In two dimensions the DFT is defined by the pair of equations

$$Z\left(k_x, k_y\right) = \begin{cases} \sum_{n_x=0}^{N_x-1} \sum_{n_y=0}^{N_y-1} z\left(n_x, n_y\right) e^{-i(2\pi/N_x)k_x n_x} e^{-i(2\pi/N_y)k_y n_y}, & 0 \leqslant k_x \leqslant N_x - 1, 0 \leqslant k_y \leqslant N_y - 1 \\ 0, & \text{otherwise} \end{cases} \tag{37a}$$

$$z\left(n_x, n_y\right) = \begin{cases} \sum_{k_x=0}^{N_x-1} \sum_{k_y=0}^{N_y-1} Z\left(k_x, k_y\right) e^{i(2\pi/N_x)k_x n_x} e^{i(2\pi/N_y)k_y n_y}, & 0 \leqslant n_x \leqslant N_x - 1, 0 \leqslant n_y \leqslant N_y - 1 \\ 0, & \text{otherwise} \end{cases} \tag{37b}$$

for a finite-extent first-quadrant support sequence [65].

The surface $z(\mathbf{r})$ must be purely real, which requires that $Z(\mathbf{k})$ be conjugate symmetric [65]

$$\text{real } z\left(n_x, n_y\right) \Leftrightarrow Z\left(k_x, k_y\right) = \tilde{Z}^*\left(-k_x, -k_x\right) R_{N_x \times N_y}\left(k_x, k_y\right) \,, \tag{38}$$

where $\tilde{Z}$ indicates here that the function is periodic with a period of $N_x \times N_y$,

$$\tilde{X}\left(k_x, k_y\right) = X\left(k_x + N_x, k_y\right) = X\left(k_x, k_y + N_y\right) \ \forall (N_x, N_y) \,, \tag{39}$$

and $R_{N_x \times N_y}\left(k_x, k_y\right)$ is defined by

$$R_{N_x \times N_y}\left(k_x, k_y\right) = \begin{cases} 1, & 0 \leqslant k_x \leqslant N_x, 0 \leqslant k_y \leqslant N_y \\ 0, & \text{otherwise} \end{cases} \,. \tag{40}$$

In general,

$$Z(\mathbf{k}) = |Z(\mathbf{k})| e^{2\pi i \arg Z(\mathbf{k})} = \Re\left[Z(\mathbf{k})\right] + \Im\left[Z(\mathbf{k})\right] \tag{41}$$

where $P(\mathbf{k}) = |Z(\mathbf{k})|^2$. Here, $z(\mathbf{r})$ is isotropic such that $Z(\mathbf{k})$ is a function of $k = \sqrt{k_x^2 + k_y^2}$ only. The square magnitude of $Z(\mathbf{k})$ is chosen to follow a modified power-law form, as given by Sec. II B. The phase is chosen to be random, though must be specified such that it meets the symmetry requirements of Eq. (38). Defining α as an antisymmetric array of random numbers uniformly distributed on $(0, 1)$ (as described in the Appendix B) yields a simple algorithm for generating a realization of the surface:

$$z(\mathbf{r}) = \mathcal{F}\left[\sqrt{P(k)}e^{2\pi i \alpha}\right] , \tag{42}$$

where $\mathcal{F}$ denotes the Fourier transform operator. While this algorithm ensures, by construction, that the expected value of the PSD of the generated surface is $P(k)$, it does not explicitly ensure that the resulting rough surface will be a realization of a Gaussian random process.

A similar approach to generate realizations of band-limited FBM, which was followed by Thorsos [66], produces realizations for which the expected value of the PSD is $P(k)$, and which also have surface-height distributions that are guaranteed to be Gaussian. In this method, $z(\mathbf{r})$ is generated by the algorithm

$$z(\mathbf{r}) = \mathcal{F}\left[\sqrt{P(k)}\frac{\mu + i\eta}{\sqrt{2}}\right] , \tag{43}$$

where μ and η are uncorrelated arrays of random numbers normally distributed with mean of zero and standard deviation of one.

An equivalent algorithm to that given in Eq. (43), which was used here, can be obtained by modifying Eq. (42) such that the magnitude is randomly distributed about $P(k)$ according to a Rayleigh distribution

$$z(\mathbf{r}) = F\left[\sqrt{-\ln(\beta) P(k)}e^{2\pi i \alpha}\right] , \tag{44}$$

where β is a symmetric array of random numbers uniformly distributed on $(0, 1)$ (as described in the Appendix B).

The Fourier transform used by these algorithms is a one-to-one linear transformation (though it is not shift-invariant). It can be shown that a linear transformation of a realization of a Gaussian random process yields a sequence that is also a realization of a Gaussian random process (Ref. 67, pp. 340-341). Consequently, a random process that is Gaussian distributed must have a Fourier transform (k-space representation) that is also Gaussian distributed in both its real and imaginary components [68]. The algorithm given in Eqs. (43) and (44) therefore yields rough surfaces that, by construction, are realizations of a Gaussian random process. In contrast, the algorithm given in Eq. (42), yields rough surfaces that are approximately realizations of a Gaussian random process through the Central Limit Theorem. The inverse DFT, Eq. (37b), of a random complex-valued random process in k space represents each sample of the transformed process in real space as a linear combination of random variables, that is, the individual samples of the k-space representation. Provided that these random variables are mutually independent with zero means and finite variances (Ref. 67, pp. 225–230), the Central Limit Theorem predicts that each sample in real space will tend toward a Gaussian distribution as the number of frequency terms in the inverse DFT becomes large. While the Central Limit Theorem is often approximately valid for surprisingly small numbers of random variables, the breakdown of the model can be aggravated by the power-law form of the PSD, which, by decreasing amplitude at large k effectively eliminates the influence of large-k terms. By using the algorithm given in Eqs. (43) and (44), the realization effectively simulates a larger surface. However, it can be argued that Eq. (42) is more representative of the central-limit processes through which physical surfaces arrive at a Gaussian height distribution.

20

B. Manufacturing Rough Surfaces

Various approaches have been followed for the manufacture scale-model rough surfaces for use in acousti-cal experiments. There is likewise a diversity of sources of fabricated topography, some electing to reproduce, at scale, topography measured from actual surfaces and others choosing to generate arbitrary surfaces sat-isfying certain statistical conditions.

In the first reported work of this type, Proud *et al.* [69] built an approximately Gaussian rough surface from layers of cork strip fixed to plywood substrate. Later Horton *et al.* [70] manufactured surfaces from low-density expanded polystyrene based on aeromagnetic contours of the Canadian Shield. Though not detailed, such a machining process must have been quite difficult given the state of the art at the time (1967). Much more recently, Gautier and Gibert [36] used resin printing to create a replica of a natural fracture surface of granite, the topography of which was measured using laser profilometry.

A particularly promising technique, which was adopted for the work described here, is use of computer-aided manufacturing (CAM) to shape surfaces of near arbitrary topography from blocks of raw material. Use of this fabrication technique for acoustical scale models was first described by Mellema (Ref. 71, pp. 33–35), but was used earlier to fabricate rough surfaces for other purposes [72, 73]. Computer-aided manufacturing uses software to develop fabrication strategies directly from computer representations of a desired finished object. Such machining strategies take the form of a series of tool paths that describe how a particular sequence of cutting tools must be moved in order to achieve a prescribed result. Tool paths are expressed in a scripting language (e.g., G code) and provide the instruction sets used by computer-numerically controlled (CNC) tools, such as milling machines.

Milling machines are described by the number of independent axes through which they can move a cutting tool. The number of axes determines the maximum Euclidean dimension (d) of the space embedding an object that such a mill is able to fabricate. Manufacture of random-rough surface topography ($\mathfrak{d} = 2, d = 3$) as described in Sec. II A requires a 3-axis mill able to independently move along each of the Cartesian axes. Additional axes, such as employed in 5-axis mills [74], are required only to fabricate objects of higher topological dimension or surfaces that are not single-valued mappings.

Machining of profiled surfaces is typically performed with a ball-nose end mill, as opposed to the more common flat end mill. Complete fidelity in milling topography $z(\mathbf{r})$ requires that ϖ, the radius of the ball-nose end mill, be smaller than $\check{\rho}$, the minimum positive radius of curvature of the surface. At any given point $\mathbf{r}$, the radius of curvature $\rho(\mathbf{r})$ is found by first calculating the mean curvature $\kappa_H(\mathbf{r})$ and the Gaussian curvature $\kappa_K(\mathbf{r})$ via

$$\kappa_H(\mathbf{r}) = \frac{\left(1 + z_y^2\right) z_{xx} - 2 z_x z_y z_{xy} + \left(1 + z_x^2\right) z_{yy}}{2 \left(1 + z_x^2 + z_y^2\right)^{3/2}} \ , \tag{45a}$$

$$\kappa_K(\mathbf{r}) = \frac{z_{xx} z_{yy} - z_{xy}^2}{\left(1 + z_x^2 + z_y^2\right)^2} \leqslant \kappa_H(\mathbf{r})^2 \ , \tag{45b}$$

where subscripts in these expressions indicate partial derivatives with respect to the coordinate axes x and y, evaluated at $\mathbf{r}$. In terms of these, $\kappa_{+,-}(\mathbf{r}) = \kappa_H(\mathbf{r}) \pm \sqrt{\kappa_H^2(\mathbf{r}) - \kappa_K(\mathbf{r})}$ are the two principal curvatures of z at $\mathbf{r}$. The minimum positive radius of curvature at $\mathbf{r}$ is $\rho(r) = 1/\kappa_+(\mathbf{r})$, such that $\check{\rho} = 1 \big/ \max_{\mathbf{r}} [\kappa_+(\mathbf{r})]$.

While easily expressed, the above requirements pose the problem of differentiating a fractal surface that, by definition, is nondifferentiable. This problem is removed in practice because the fractal surface is given a discrete, finite-support (and therefore band-limited) representation that is only approximately self-affine. Consequently, derivatives are defined [19, 24].

The requirement of fidelity limits the maximum radius of the tool used to mill the surface, but the nec-
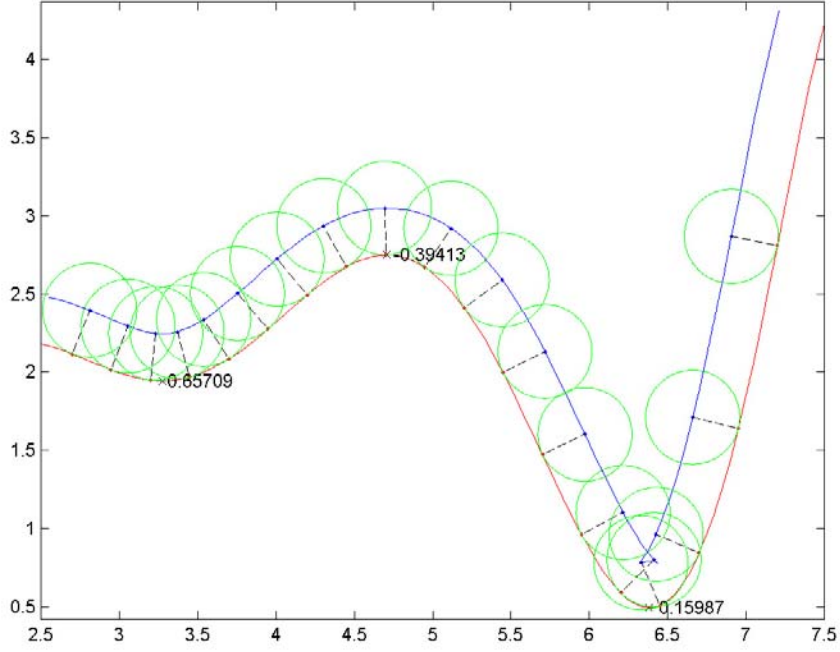
FIG. 9: Simulation of a ball-nose end mill tracing the evolute tool path.

essarily small cutting-edge length of such a tool may be inconsistent with the relief depth of the topography to be milled. As a result, milling may require a process of many steps; each step removing a thickness of material less than the cutting-edge length of the tool. A process based on use of a single tool capable of resolving all features of the topography would be too inefficient for practical use. Instead, a multistep process is followed in which the size of the tool is progressively decreased with each cutting pass. Such a process is typically categorized into two stages of milling operations: roughing and finishing.

In the roughing stages, one or more flat end mills are used to remove excess material from areas where no detailed profiling of the surface is required. Various strategies may be followed in preparing the surface for finishing [75]. One class of method removes excess material by machining a series of offset surfaces of increasing fidelity. Once a sufficient amount of material has been removed, the remaining detailing is completed during finishing stages. An alternative method, used here, divides the surface into a number of equal-height contours and removes material sequentially from each layer. The resulting terraced surface is sculpted into the desired form during the finishing stages.

In the finishing stages, one or more ball-nose end mills are used to cut increasingly detailed surfaces. During each finishing stage, a surface derived from the desired topography, but having a level of detail appropriate to the cutter radius used, is milled. In the final finishing stage, the smallest cutter, having $\varpi < \check{\rho}$, is used to mill the desired topography.

In order to machine the surface accurately, without removing excess surface material, the center point of the spherical tip of the end mill must be offset from the surface by ϖ in the direction of the outward local normal vector to the surface [74]. Equivalently, this can be expressed as the condition that the center point of a ball-nose end mill of tip radius ϖ moves in the ϖ-evolute surface associated with the desired rough surface. This is illustrated in Fig. 9. Note that the evolute surface allows for accurate machining

22

only where $\varpi < \check{\rho}$. In the case where $\varpi \geq \check{\rho}$ the evolute surface is no longer single valued and gouging occurs. Typically, the tool path consists of a series of tool passes: closely spaced profiles along the evolute surface, which the cutter is made to raster across in the process of machining the surface. The final fidelity
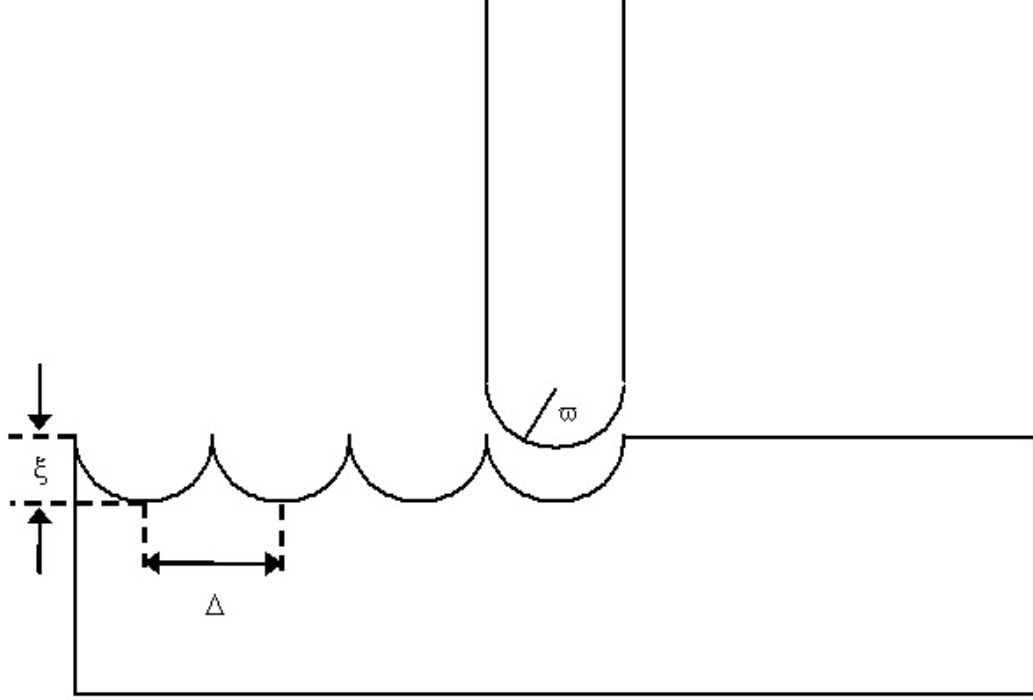

FIG. 10: A schematic representation of scalloping caused by by machining a surface with a ball-nose end mill.

of the finishing stage is determined not only by the smallest tip-radius of ball-nose end mill used, but also by the tool-pass interval, which is the nominal linear spacing between adjacent profiles followed by the cutter. An ideal ball-nose end mill moving on an ideal evolute surface for which $\varpi < \check{\rho}$ contacts $z(\mathbf{r})$ only on the profiles (tool passes) comprising the tool path. Consequently, for any finite tool pass interval, the finishing stage leaves excess material on the surface, as shown in Fig. 10. The height of these so-called scallops is determined by the tool-pass interval, the tip radius of the ball-nose end mill, and the local topography of $z(\mathbf{r})$ [73, 74]. For a flat surface, the scallops are of uniform height $\xi = \varpi - \sqrt{\varpi - (\Delta/2)^2}$, where Δ is the tool-pass interval. The primary requirement, after fidelity, is scallops of a sufficiently small size that neither the collective effect of isolated scattering from single scallops nor the effect of the grating scattering resulting from their aggregate are significant in the frequency range of interest.

An example of a rough surface physically realized using the techniques described here is shown in Figs. 11–12. In Fig. 11, the desired topography is shown and compared with the topography of the realized sample as measured by a touch-trigger probe, shown in Fig. 12. The maximum difference between these two measured topographies is ≤ 1 mm.
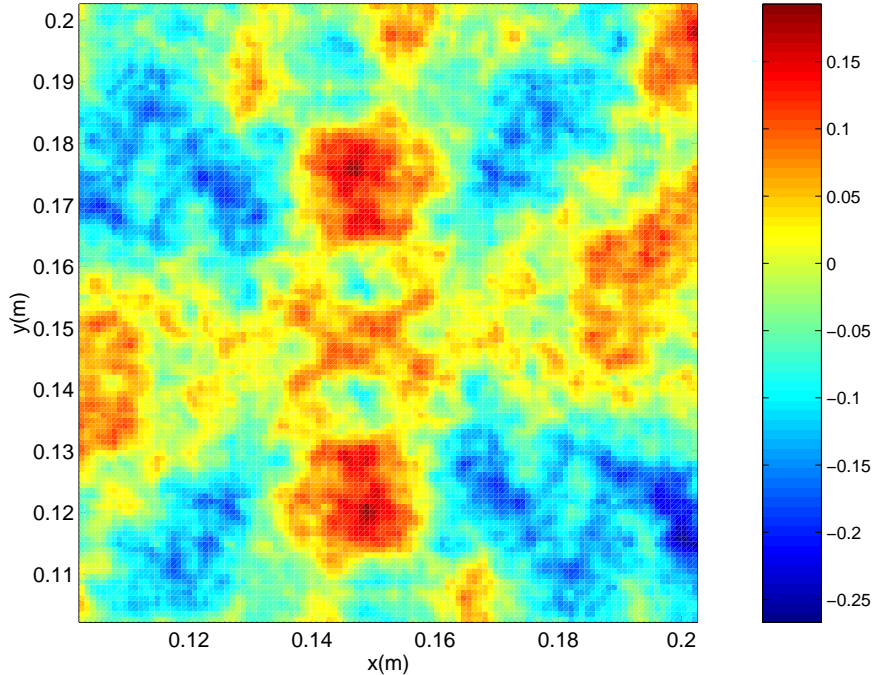
FIG. 11: Topography of a computer-generated realization of band-limited FBM.

C. Verifying Properties of Rough-Surface Realizations

Measurement and characterization of physical realizations of band-limited FBM and other random rough surfaces are needed both to confirm that manufactured physical realizations have achieved the desired form and to characterize existing rough surfaces.

1. Measurement

Reviews of techniques for measurement of rough-surface topography can be found in Refs. 76 and 7. Many sophisticated techniques exist, but simple contact methods are sufficient to characterize surface topography over length scales relevant for acoustical scattering. Such methods include traditional stylus methods (profilometry) as described in Ref. [76] and the modern and conceptually simple kinematic-resistive touch-trigger probe used in coordinate measurement machines (CMMs) [77, 78, 79].

For the work described here, a touch-trigger probe was used. Unlike profilometric methods that provide a continuous reporting of surface height, touch-trigger probes specify surface coordinates at discrete points. For rough surfaces this translates to specification of the surface height at discrete points on a uniform two-dimensional grid, a representation termed a digital elevation model (DEM). This representation is analogous to that used for the numerical generation of rough surface topography described in Sec. III A, and therefore
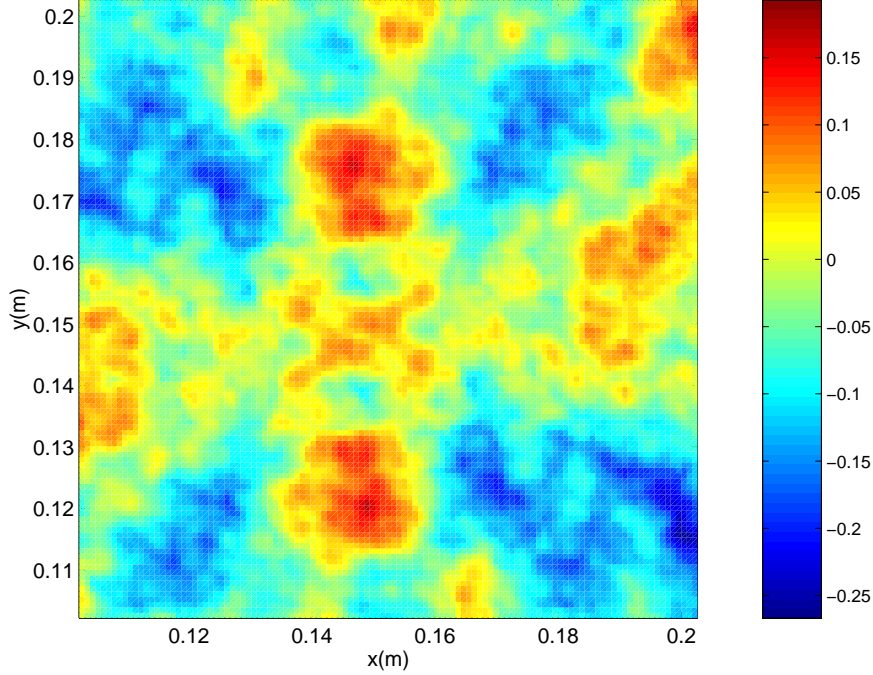
24

FIG. 12: Topography of a physical realization manufactured from the numerical realization shown in Fig. 11 as measured by a touch-trigger probe.

has the same large-k cutoff described in Sec. III A 1.

Similarly, the tip radius of the touch-trigger probe must meet the criteria given in Sec. III B in order to accurately represent the surface topography. If the tip radius ϖ does not satisfy $\varpi < \check{\rho}$, the touch-trigger probe will report truncated depths for those valleys where $\varpi > \rho$. This effect of the spherical radius of the probe is similar to that of a low-pass wavenumber filter applied to the topography [80, 81].

Data obtained by physical measurement commonly contain errors in the form of piston or tilt (equivalent to biases of $\mathfrak{d} = 1$ profiles described by zeroth- or first-order polynomials, respectively) due to misalignment between the surface and the measuring machine. This can be removed by fitting a plane to the surface and then subtracting this plane from the measured DEM. The resulting detrended data have a modified PSD, as described in Sec. (II B). Additionally, detrending is appropriate only if the sample is large enough relative to the small-k cutoff of the PSD that there is no underlying bias in the topography of the sample itself.

2. Analysis

Analysis of DEMs, either numerically generated or measured from real surfaces, can serve a number of purposes. For numerically derived DEMs, analysis can determine whether a realization is representative of the ensemble from which it was drawn. For physically derived DEMs, analysis can characterize and unknown

physical surface or validate that a manufactured surface has the desired properties.

Rough-surface topography is primarily characterized by its PSD. Consequently, analysis of DEMs typically comprises spectral estimation followed by parametric descriptions of the spectral estimate, such as $w_{\mathfrak{d}}$ and $\gamma_{\mathfrak{d}}$. While many methods of spectral estimation exist (see, e.g., Ref. 82), PSDs of power-law form present certain complications [83]. Spectral estimates based on the Fourier transform of a finite-length profile suffer from spectral leakage due to convolution in k-space of the Fourier transform of the topography with the Fourier transform of the windowing function. As noted by Austin *et al.* [83], spectral leakage is a particular problem for PSDs of power-law form because leakage of high-power components at small k raises the estimated power of components at large k resulting in an overall bias of the spectral estimate toward PSD of shallower slope. This results in underestimation of $\gamma_{\mathfrak{d}}$ and overestimation of $w_{\mathfrak{d}}$.

Use of spatial windows having rapidly decaying Fourier transforms can partially address this, but only at the expense of decreased spectral resolution. Alternatively, DEMs can be prewhitened before spectral estimation in order to reduce spectral leakage and the estimated PSD corrected by a multiplicative factor to account for prewhitening [8, 13, 26, 83]. Prewhitening is easily achieved by taking the first differences of the data [8, 26].

An alternative to spectral characterization of DEMs is characterization in terms of fractal parameters H and τ. While fractal parameters are typically estimated from PSD, they can also be estimated by nonspectral methods. This is necessary in the case of DEM because their inherent band limiting causes the relationship between H and $\gamma_{\mathfrak{d}}$ to break down [49, 50, 53].

IV. SUMMARY

The rough topography of an ocean bottom can be modeled as an isotropic two-dimensional random field having a power spectral density of power-law form. While idealized random fields having power spectral density of this form are self-affine stochastic fractals (realizations of FBM), manufacturing constraints impose high- and low-k cutoffs on the power-law form of the PSD. As a result, physically realized scale models of ocean bottoms are approximately self-affine surfaces (realizations of band-limited FBM) for which scaling properties exist only over a finite hierarchy of scales and conventional relations between PSD and fractal geometry break down. Rather than serve as a complication, the breakdown of the idealized fractal model produces meaningful relations between concepts from fractal geometry and conventional statistical metrics. These new relations explicitly involve wavenumber cutoffs, which, as shown in Sec. II D, are as influential on the appearance of fractal surfaces as the parameters describing the PSD.

Discretely sampled realizations of band-limited FBM can be numerically generated by Fourier-transform methods, with high- and low-k cutoff corresponding to sampling interval and array size, respectively. Physical realizations of these numerical representations can be accurately manufactured by CAM techniques using a CNC milling machine under the condition that the tip radius of the ball-nose end mill used for the final finishing is smaller than the minimum positive radius of curvature of the surface.

In this report the recent concept of approximately self-affine profiles and surfaces has been newly introduced into the context of modeling the rough topography of the ocean bottom and the fabrication of physical models. Although physical realizations of FBM have been previously fabricated [71, 72], prior work has not considered the effects of the band-limiting imposed by the fabrication process on the fractal properties of the resulting physical realization. It has been shown that, given restrictions in bandwidth, the parameters of the power-law spectrum typically used in the field of underwater acoustics to characterize the surface, are no longer simply related to the more fundamental description of the surface in terms of fractal geometry. Moreover, as Sec. II D illustrates, the location of the low-k cutoff can markedly affect even the appearance

of approximately self-affine band-limited FBM. Additionally, this report has given algorithms for numerical generation of surface topography of this type and guidelines for CAM that are specific to this topography. The discussion concerning numerical generation contributes a more explicit clarification of the differences between previously published spectral methods.

Acknowledgments

APPENDIX A: REALIZATIONS OF BAND-LIMITED FRACTAL SURFACES

This appendix contains the still frames of the embedded movie in Fig. 3, as described in Table I.

FIG. 13: Realization of a band-limited fractal surface with $w_2 = 1 \cdot 10^{-5}$ m^4, $\gamma_2 = 2.0$, and $ka_L = 0.05$. (See Table I.)
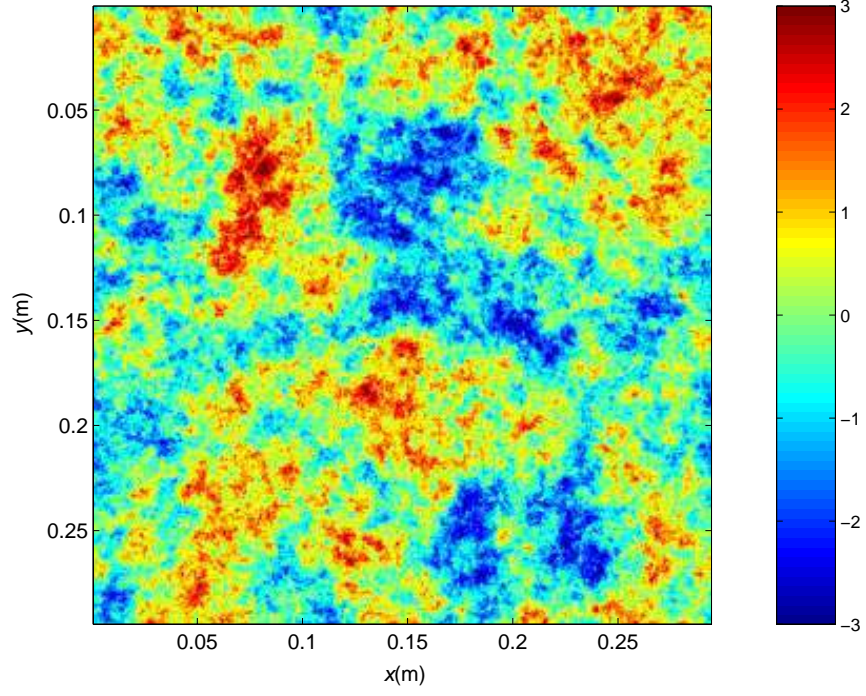
FIG. 14: Realization of a band-limited fractal surface with $w_2 = 1 \cdot 10^{-5}$ m^4, $\gamma_2 = 2.4$, and $ka_L = 0.05$. (See Table I.)
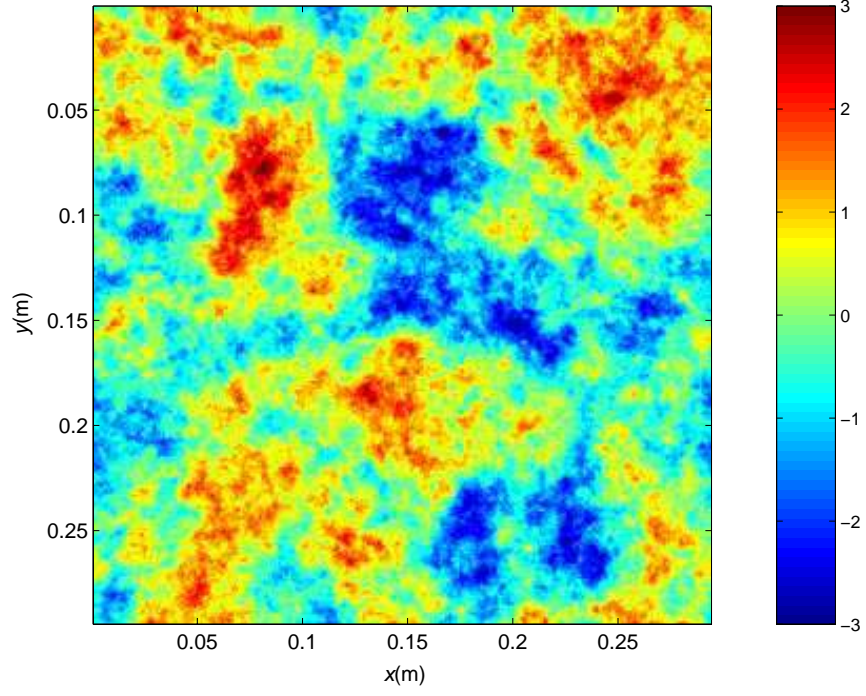
FIG. 15: Realization of a band-limited fractal surface with $w_2 = 1 \cdot 10^{-5}$ m^4, $\gamma_2 = 2.8$, and $ka_L = 0.05$. (See Table I.)

FIG. 16: Realization of a band-limited fractal surface with $w_2 = 1 \cdot 10^{-5} \text{ m}^4$, $\gamma_2 = 3.2$, and $ka_L = 0.05$. (See Table I.)

FIG. 17: Realization of a band-limited fractal surface with $w_2 = 1 \cdot 10^{-5}$ m^4, $\gamma_2 = 3.6$, and $ka_L = 0.05$. (See Table I.)
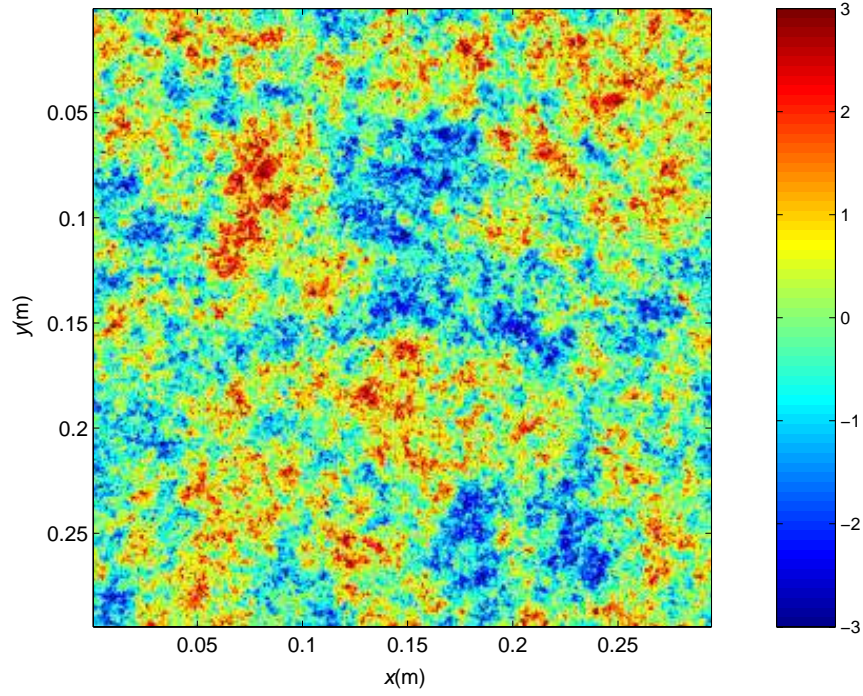
FIG. 18: Realization of a band-limited fractal surface with $w_2 = 1 \cdot 10^{-5}$ m^4, $\gamma_2 = 4.0$, and $ka_L = 0.05$. (See Table I.)

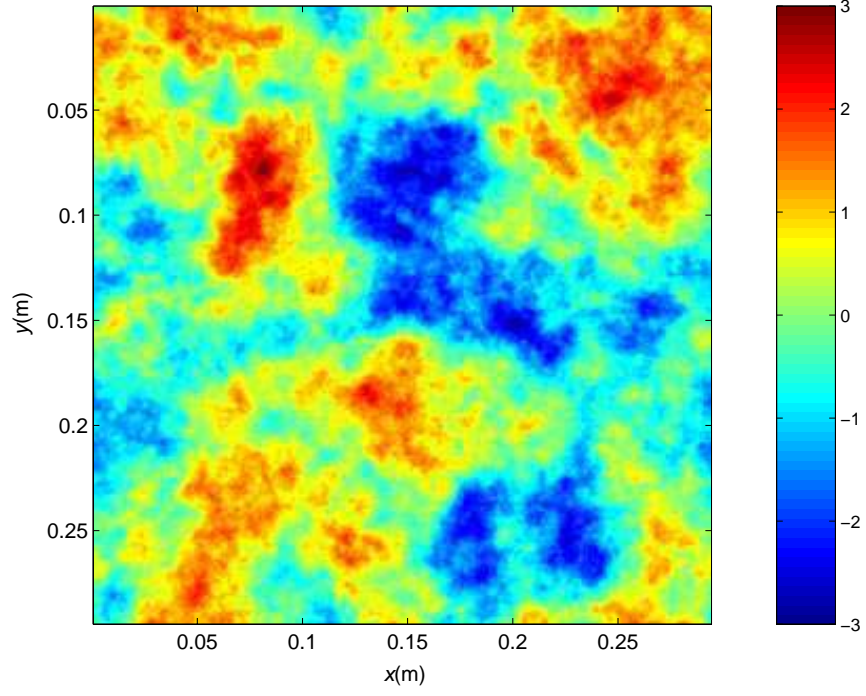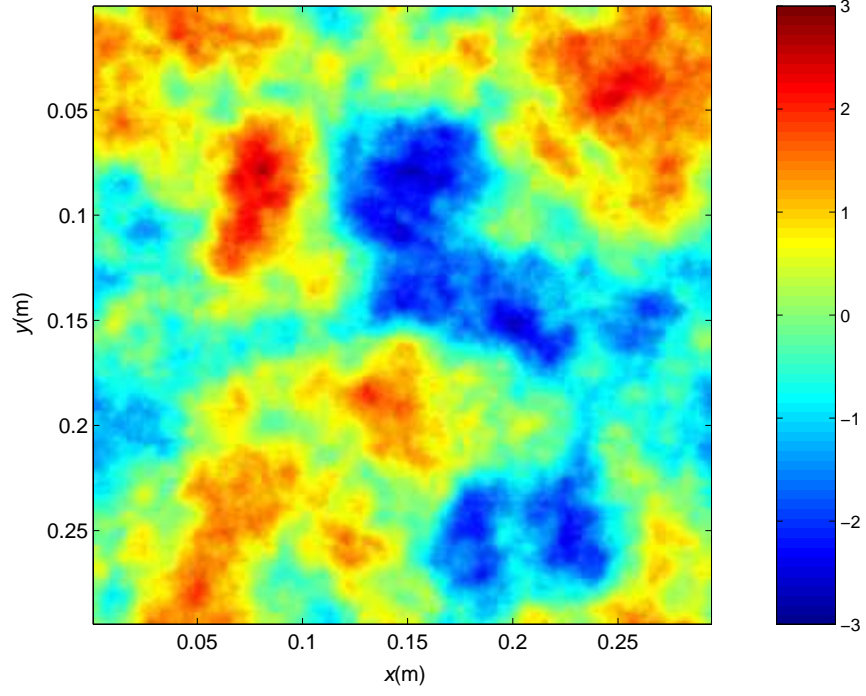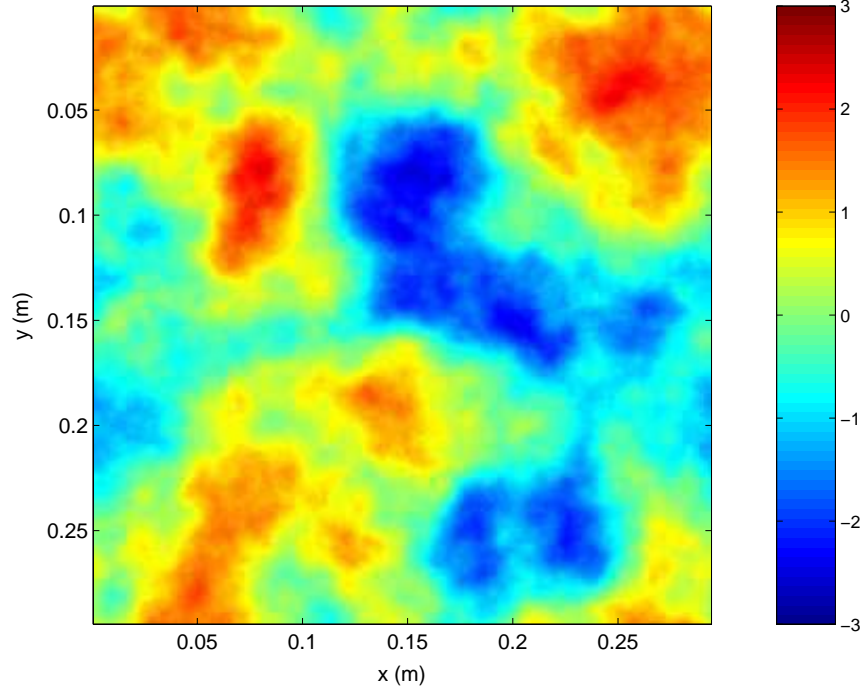## APPENDIX B: DETAILS OF ALGORITHM FOR GENERATION OF SURFACE REALIZATIONS

Because $z(\mathbf{r})$ is real, $Z(\mathbf{k})$ must be conjugate symmetric. Efficient computation of $z(\mathbf{r})$ from $Z(\mathbf{k})$ by the DFT using the FFT algorithm requires that the matrices have dimensions that are integer powers of two. A conjugate symmetric M by N matrix where both M and N are even is of the form

$$
\begin{bmatrix}
a_{1,1} & a^*_{1,N} & a^*_{1,N-1} & \cdots & a^*_{1,\frac{N}{2}+2} & a_{1,\frac{N}{2}+1} & \cdots & \cdots & a_{1,N} \\
a_{1,2} & a^*_{M,N} & a^*_{M,N-1} & \cdots & a^*_{M,\frac{N}{2}+2} & \vdots & \ddots & & \vdots \\
\vdots & \vdots & & & \vdots & \vdots & & \ddots & \vdots \\
a_{\frac{M}{2}+1,1} & \vdots & \ddots & & \vdots & a_{\frac{M}{2}+1,\frac{N}{2}+1} & \cdots & \cdots & \vdots \\
a^*_{\frac{M}{2},1} & \vdots & & \ddots & \vdots & a^*_{\frac{M}{2},\frac{N}{2}+1} & a_{\frac{M}{2}+2,\frac{N}{2}+2} & \cdots & \vdots \\
\vdots & \vdots & & & \vdots & \vdots & \vdots & \ddots & \vdots \\
a^*_{2,1} & a^*_{2,N} & a^*_{2,N-1} & \cdots & a^*_{2,\frac{N}{2}+2} & a^*_{2,\frac{N}{2}+1} & a_{M,\frac{N}{2}+2} & \cdots & a_{M,N}
\end{bmatrix},
\tag{B1}
$$

where the subscripts indicate the row and column, respectively. In those cases where the indices appear to be incorrect, it simply represents the conjugate symmetry of the matrix. The matrix of uniformly distributed random numbers α used in Eqs. (42 and 44) must have odd symmetry, as illustrated by the antisymmetric matrix below

$$
\begin{bmatrix}
a_{1,1} & -a_{1,N} & -a_{1,N-1} & \cdots & -a_{1,\frac{N}{2}+2} & a_{1,\frac{N}{2}+1} & \cdots & \cdots & a_{1,N} \\
a_{1,2} & -a_{M,N} & -a_{M,N-1} & \cdots & -a_{M,\frac{N}{2}+2} & \vdots & \ddots & & \vdots \\
\vdots & \vdots & & & \vdots & \vdots & & \ddots & \vdots \\
a_{\frac{M}{2}+1,1} & \vdots & \ddots & & \vdots & a_{\frac{M}{2}+1,\frac{N}{2}+1} & \cdots & \cdots & \vdots \\
-a_{\frac{M}{2},1} & \vdots & & \ddots & \vdots & -a_{\frac{M}{2},\frac{N}{2}+1} & a_{\frac{M}{2}+2,\frac{N}{2}+2} & \cdots & \vdots \\
\vdots & \vdots & & & \vdots & \vdots & \vdots & \ddots & \vdots \\
-a_{2,1} & -a_{2,N} & -a_{2,N-1} & \cdots & -a_{2,\frac{N}{2}+2} & -a_{2,\frac{N}{2}+1} & a_{M,\frac{N}{2}+2} & \cdots & a_{M,N}
\end{bmatrix}.
\tag{B2}
$$

In contrast, the matrix of uniformly distributed random numbers β used in Eq. (44) must have even symmetry, as illustrated by the symmetric matrix below

$$
\begin{bmatrix}
a_{1,1} & a_{1,N} & a_{1,N-1} & \cdots & a_{1,\frac{N}{2}+2} & a_{1,\frac{N}{2}+1} & \cdots & \cdots & a_{1,N} \\
a_{1,2} & a_{M,N} & a_{M,N-1} & \cdots & a_{M,\frac{N}{2}+2} & \vdots & \ddots & & \vdots \\
\vdots & \vdots & & & \vdots & \vdots & & \ddots & \vdots \\
a_{\frac{M}{2}+1,1} & \vdots & \ddots & & \vdots & a_{\frac{M}{2}+1,\frac{N}{2}+1} & \cdots & \cdots & \vdots \\
a_{\frac{M}{2},1} & \vdots & & \ddots & \vdots & a_{\frac{M}{2},\frac{N}{2}+1} & a_{\frac{M}{2}+2,\frac{N}{2}+2} & \cdots & \vdots \\
\vdots & \vdots & & & \vdots & \vdots & \vdots & \ddots & \vdots \\
a_{2,1} & a_{2,N} & a_{2,N-1} & \cdots & a_{2,\frac{N}{2}+2} & a_{2,\frac{N}{2}+1} & a_{M,\frac{N}{2}+2} & \cdots & a_{M,N}
\end{bmatrix}.
\tag{B3}
$$

APPENDIX C: MATLAB FUNCTIONS

This appendix contains the header portions of MATLAB functions used to numerically generate and characterize band-limited FBM. The full functions along with required support functions are included on this CD-ROM. The MATLAB functions were developed under MATLAB 6.1 R12 and, in some cases, require the Signal Processing Toolbox (or equivalent functions written by the user) for operation. All software on this CD-ROM is distributed freely, but is subject to the copyrights and terms of use specified in the headers of the individual files.

1. Numerical generation of band-limited FBM surfaces

```
function surf_z=generate_surface(varargin)

% []=generate_surface(frq,c,Lx,Ly,dx,dy,spectratype,w_2_gamma_2,
%                     LF_param,pname,randstate)
%
% Generates a 2-D random rough surface with a power-law spectrum
% and low-frequency roll-off.  The surface and parameters are saved
% to a file.  Plots of the surface can be displayed.
%
% If called as a function with input parameters, the parameters
% specified in the function call are used instead of the
% parameters specified in the file and plotting is disabled.
%
% J.E. Summers, 2005

%%%%%%%%%%%%%%%%%%%%%%%%%%%%%%%%%%%%%%%%%%%%%%%%%%%%%%%%%%%%%%%%%%%%%%%%%
% Reference
%%%%%%%%%%%%%%%%%%%%%%%%%%%%%%%%%%%%%%%%%%%%%%%%%%%%%%%%%%%%%%%%%%%%%%%%%
%
% J. E. Summers, R. J. Soukup, and R. F. Gragg, "Characterization
% and fabrication of synthetic rough surfaces for acoustical scale
% -model experiments," NRL/MR-MM/7140--05-8871, U. S. Naval Research
% Laboratory, Washington, D.C., 2005
%
%%%%%%%%%%%%%%%%%%%%%%%%%%%%%%%%%%%%%%%%%%%%%%%%%%%%%%%%%%%%%%%%%%%%%%%%%

%%%%%%%%%%%%%%%%%%%%%%%%%%%%%%%%%%%%%%%%%%%%%%%%%%%%%%%%%%%%%%%%%%%%%%%%%
%%%%%%%%%%%%%%%%%%%%%%%%%%%%%%%%%%%%%%%%%%%%%%%%%%%%%%%%%%%%%%%%%%%%%%%%%
% Conditions and terms for the use of this software
%
% This software may be used, reproduced, modified, and distributed
% by the user for noncommercial purposes but is Copyright (C)
% Jason E. Summers (summers@abyss.nrl.navy.mil).
%
% Users have the right to use the software with the following terms
% and conditions:
%
%    Users agree that any copies of the software will contain the same
%    proprietary notices and warranty disclaimers which appear in this
%    software.
%
% Users can make modifications to this software but must
%    include references to the original software and author.
%
% If a user makes any modifications to this software and the
%    modified software is redistributed, then the user must notify the
%    author of the original software by an e-mail sent to
%    summers@abyss.nrl.navy.mil.
%
% The original author shall be credited should this software be used
%    in any form or written about in any publication.
%
% This software is provided "as is", without warranty by the author
%    or by the United States Naval Research Laboratory (NRL). Although
%    the software has been tested on Windows machines under
%    MATLAB 6.1 R12, neither the author nor NRL make any warranties
%    relating to the software's performance on this or any other
%    platforms.  The author and NRL make no express, implied, or
%    statuatory warranty of any kind for this software including, but
%    not limited to, any warranty of performance, merchantability, or
%    fitness for a particular purpose.  In no event shall the author or
%    NRL be liable to the user or any thrid party for any loss or for
%    any indirect, special, punitive, examplary, incidental, or
%    consequential damages arising from the use, possession or
%    performance of this software, even if the author or NRL have
%    been advised of the possibility thereof.
%
% Any comments on errors, or hints about possible improvements or
% extensions are appreciated.
%%%%%%%%%%%%%%%%%%%%%%%%%%%%%%%%%%%%%%%%%%%%%%%%%%%%%%%%%%%%%%%%%%%%%%%%%

%%%%%%%%%%%%%%%%%%%%%%%%%%%%%%%%%%%%%%%%%%%%%%%%%%%%%%%%%%%%%%%%%%%%%%%%%
%%%%%%%%%%%%%%%%%%%%%%%%%%%%%%%%%%%%%%%%%%%%%%%%%%%%%%%%%%%%%%%%%%%%%%%%%
% Dependencies
%%%%%%%%%%%%%%%%%%%%%%%%%%%%%%%%%%%%%%%%%%%%%%%%%%%%%%%%%%%%%%%%%%%%%%%%%
% requires:
% Signal Processing Toolbox: fftshift.m
% calcspectra.m : computes the 2-D roughness spectrum
% rand2.m : computes the 2-D realization
% odd.m : rounds to the nearest odd number (time-frequency toolbox)
%
% can be used with:
% characterize_surface.m : characterizes the surface and generates
%                          a text file of descriptors
% export_surface.m : exports the surface geometry into common
%                    CAD/CAM formats (*.asc, *.stl)
%%%%%%%%%%%%%%%%%%%%%%%%%%%%%%%%%%%%%%%%%%%%%%%%%%%%%%%%%%%%%%%%%%%%%%%%%

%%%%%%%%%%%%%%%%%%%%%%%%%%%%%%%%%%%%%%%%%%%%%%%%%%%%%%%%%%%%%%%%%%%%%%%%%
% Input Parameters
%%%%%%%%%%%%%%%%%%%%%%%%%%%%%%%%%%%%%%%%%%%%%%%%%%%%%%%%%%%%%%%%%%%%%%%%%

if nargin<1

% target measurement frequency (Hz)
frq = 300000;

% speed of sound (meters/sec)
% GPM RSS2: 1482 m/s
c = 1482;

% desired surface dimensions (meters)
Lx = 1;
Ly = 1;

% desired spacing between sample points (meters)
dx = 1e-3;
dy = 1e-3;

% form of the spectrum
spectratype='alg';
%            * 'moe': Moe's spectrum (Gaussian LF cutoff) [Eq. (15)]
%            * 'pwr': power law [Eq. (10)]
%            * 'alg': power law with algebraic LF cutoff [Eq. (13)]
%            * 'box': power law with box-car HF and LF cutoff [Eq. (12)]
%            * 'dif': power law with LF cutoff expressed as the
%                     difference of two pure power laws [Eqs. (16)]

% for the realization either the inverse transform of the roughness
% spectrum can be done by assuming random phases with a Gaussian
% distribution only (amprand=0) or by adding a random amplitude
% factor given by a Rayleigh distribution (amprand=1)
amprand=1;

% spectral strength (meters^4)
w_2 = 2.0e-5;

% two-dimensional spectral exponent
% (dimensionless number between 2 and 4)
gamma_2 = 3.5;

% low-frequency cutoff parameter
LF_param = 20;
% try 0.05 for a in moe (knee at K~30; scales in K linearly with
%                        1/LF_param)
% try 20 for mod

%path name in which to save created surface
pname='D:\NRL\';

% number of the random iteration to create
```

```
% (0 to 2^1492, which is the period of Matlab's internal
%  random number generator)
randstate=333;

% turn on and off plotting
plotsurf=0; % 1 to show plots, 0 to not
plotspec=0; % 1 to show plots of spectrum, 0 to not

elseif nargin==12

frq=varargin{1};
c=varargin{2};
Lx=varargin{3};
Ly=varargin{4};
dx=varargin{5};
dy=varargin{6};
spectrtype=varargin{7};
```

```
w_2=varargin{8};
gamma_2=varargin{9};
LF_param=varargin{10};
pname=varargin{11};
randstate=varargin{12};

else

error('generate_surface: wrong number of input arguments')

end

%%%%%%%%%%%%%%%%%%%%%%%%%%%%%%%%%%%%%%%%%%%%%%%%%%%%%%%%%%%%%%%%%%%%%%%%%%%%
```

2.   Characterization of discrete-sampled rough surfaces

```
function varargout=characterize_surface(varargin)

% [w_2,gamma_2]=characterize_surface(Spname,Sfname)
%
% Where Spname and Sfname are the path name and file name of a file
% created by generate_surface.m.
%
% or
%
% [w_2,gamma_2]=characterize_surface(c,dx,dy,surf_z,frq)
%
% Where c is the sound speed, dx is sample spacing in x, dy is the
% sample spacing in y, and surf_z is a matrix of surface heights.
%
% or
%
% [w_2,gamma_2]=characterize_surface(c,surf_x,surf_y,surf_z,frq)
%
% Where c is the sound speed, surf_x is a matrix of x coordinates,
% surf_y is a matrix of y coordinates, and surf_z is a matrix of
% surface heights.
%
% Calculates parameters of a 2D random rough surface with a power-law
% spectrum, which are then displayed on the screen and output to a
% text file.  The following parameters are calculated:
%
% max and min surface height
% rms surface height
% minimum curvature
% smallest ball-nose end mill required to mill surface accurately
% correlation length
% w_2
% gamma_2
% fractal dimension
% Hurst exponent
% topothesy
%
% If called as a function, plotting and screen displays are disabled.
%
% If called with no outputs, results are displayed on screen and
% plotted.
%
% If called with no inputs, a default file is opended and analyzed.
%
% J.E. Summers, 2005

%%%%%%%%%%%%%%%%%%%%%%%%%%%%%%%%%%%%%%%%%%%%%%%%%%%%%%%%%%%%%%%%%%%%%%%%%%%%
% Reference
%%%%%%%%%%%%%%%%%%%%%%%%%%%%%%%%%%%%%%%%%%%%%%%%%%%%%%%%%%%%%%%%%%%%%%%%%%%%
%
% J. E. Summers, R. J. Soukup, and R. F. Gragg, "Characterization
% and fabrication of synthetic rough surfaces for acoustical scale
% -model experiments," NRL/MR-MM/7140--05-8871, U. S. Naval Research
% Laboratory, Washington, D.C., 2005
%
%%%%%%%%%%%%%%%%%%%%%%%%%%%%%%%%%%%%%%%%%%%%%%%%%%%%%%%%%%%%%%%%%%%%%%%%%%%%

%%%%%%%%%%%%%%%%%%%%%%%%%%%%%%%%%%%%%%%%%%%%%%%%%%%%%%%%%%%%%%%%%%%%%%%%%%%%
%%%%%%%%%%%%%%%%%%%%%%%%%%%%%%%%%%%%%%%%%%%%%%%%%%%%%%%%%%%%%%%%%%%%%%%%%%%%
% Conditions and terms for the use of this software
%
% This software may be used, reproduced, modified, and distributed
% by the user for noncommercial purposes but is Copyright (C)
% Jason E. Summers (summers@abyss.nrl.navy.mil).
%
% Users have the right to use the software with the following terms
% and conditions:
%
```

```
%   Users agree that any copies of the software will contain the same
%   proprietary notices and warranty disclaimers which appear in this
%   software.
%
% Users can make modifications to this software but must
%   include references to the original software and author.
%
% If a user makes any modifications to this software and the
%   modified software is redistributed, then the user must notify the
%   author of the original software by an e-mail sent to
%   summers@abyss.nrl.navy.mil.
%
% The original author shall be credited should this software be used
%   in any form or written about in any publication.
%
% This software is provided "as is", without warranty by the author
%   or by the United States Naval Research Laboratory (NRL). Although
%   the software has been tested on Windows machines under
%   MATLAB 6.1 R12, neither the author nor NRL make any warranties
%   relating to the software's performance on this or any other
%   platforms.  The author and NRL make no express, implied, or
%   statuatory warranty of any kind for this software including, but
%   not limited to, any warranty of performance, merchantability, or
%   fitness for a particular purpose.  In no event shall the author or
%   NRL be liable to the user or any thrid party for any loss or for
%   any indirect, special, punitive, examplary, incidental, or
%   consequential damages arising from the use, possession or
%   performance of this software, even if the author or NRL have
%   been advised of the possibility thereof.
%
% Any comments on errors, or hints about possible improvements or
% extensions are appreciated.
%%%%%%%%%%%%%%%%%%%%%%%%%%%%%%%%%%%%%%%%%%%%%%%%%%%%%%%%%%%%%%%%%%%%%%%%%%%%
%%%%%%%%%%%%%%%%%%%%%%%%%%%%%%%%%%%%%%%%%%%%%%%%%%%%%%%%%%%%%%%%%%%%%%%%%%%%

%%%%%%%%%%%%%%%%%%%%%%%%%%%%%%%%%%%%%%%%%%%%%%%%%%%%%%%%%%%%%%%%%%%%%%%%%%%%
% Dependencies
%%%%%%%%%%%%%%%%%%%%%%%%%%%%%%%%%%%%%%%%%%%%%%%%%%%%%%%%%%%%%%%%%%%%%%%%%%%%
% requires:
% Signal Processing Toolbox: xcorr.m
% linfit.m : a least-squares linear-fitting routine
% calc_curve.m : calculates curvature of a surface
%
% can be used with:
% generate_surface.m : generates a 2D random rough surface
%                       with a specified power-law spectrum
% export_surface.m : exports the surface geometry into common
%                       CAD/CAM formats (*.asc, *.stl)
%%%%%%%%%%%%%%%%%%%%%%%%%%%%%%%%%%%%%%%%%%%%%%%%%%%%%%%%%%%%%%%%%%%%%%%%%%%%

if nargout==1 | nargout>2

    error('characterize_surface: wrong numer of output arguments')

end

%%%%%%%%%%%%%%%%%%%%%%%%%%%%%%%%%%%%%%%%%%%%%%%%%%%%%%%%%%%%%%%%%%%%%%%%%%%%
% Input Parameters
%%%%%%%%%%%%%%%%%%%%%%%%%%%%%%%%%%%%%%%%%%%%%%%%%%%%%%%%%%%%%%%%%%%%%%%%%%%%

if nargin==0
    % file name containing the surface realization to be characterized
    Spname='D:\NRL\GeoacousticPhysicalModeling\2004\';
    Sfname='W2_1e-005_G2_3_rP_333';
    % load the surface realization data
    load([Spname Sfname '.mat'],'-mat')
    % control plotting
    plotstats=1; % 1 to show plots of statistics, 0 to not
    plotfits=0;
```

```
    normalize_plot=0; % 1 to normalize the S vs. k plots, 0 to not

elseif nargin==2

    if ischar(varargin{1})
        Spname=varargin{1};
        Sfname=varargin{2};
        % load the surface realization data
        load([Spname Sfname '.mat'],'-mat')
    end

elseif nargin==4

    if isnumeric(varargin{1})
        c=varargin{1};
        surf_z=varargin{4};
        if size(varargin{2})==[1 1]
            dx=varargin{2};
            dy=varargin{3};
        else
            surf_x=varargin{2};
            surf_y=varargin{3};
        end
    end
else

    error('characterize_surface: wrong number of input arguments')

end

%%%%%%%%%%%%%%%%%%%%%%%%%%%%%%%%%%%%%%%%%%%%%%%%%%%%%%%%%%%%%%%%%%%%%%%%%%%%
```

GLOSSARY OF SYMBOLS

CAM   Computer-aided machining.

CMM   Coordinate measurement machine.

DEM   Digital elevation model.

PDF   Power density function.

PSD   Power spectral density.

$<>_e$ Ensemble average.

$<>_s$ Spatial average.

γ_1 One-dimensional roughness exponent.

γ_2 Radial roughness exponent.

Δ Tool-pass interval.

κ_H Mean curvature.

κ_K Gaussian curvature.

κ_+ Maximum principal curvature.

κ_- Minimum principal curvature.

ξ Scallop height.

ϖ Radius of ball-nose end mill.

$\check{\rho}$ Minimum positive radius of curvature of $z(\mathbf{r})$.

$\rho(\mathbf{r})$ Radius of curvature of $z(\mathbf{r})$ at $\mathbf{r}$.

σ Root-mean-square roughness.

τ Topothesy.

B Box dimension.

C Autocorrelation.

C_0 Autocovariance.

d Euclidean dimension.

$\mathfrak{d}$ Topological dimension.

$f_z(\zeta)$ Probability density function of z.

h_0	Reference length.
H	Hausdorff-Besicovitch dimension.
J_0	Zeroth-order Bessel function.
k	Radial spatial wave number.
k_+	Upper cutoff of k.
k_-	Lower cutoff of k.
k_H	Upper cutoff of k.
k_L	Lower cutoff of k.
k_p	Location of spectral peak.
k_x	One-dimensional spatial wave number.
$\check{k}_x$	Minimum resolvable k_x.
$\hat{k}_x$	Maximum resolvable k_x.
ka_L	Lower cutoff of k.
ℓ	Correlation length.
$P(k)$	Radial power spectral density.
$\mathfrak{p}(k_x)$	Linear power spectral density.
$\mathbf{r}$	Two-dimensional vector of position with coordinates (x, y).
R	Translation $|r_1 - r_2|$.
$\mathbb{R}^n$	Set of real number in n dimensions.
$S(\mathbf{R})$	Structure function.
w_1	One-dimensional spectral strength.
w_2	Radial spectral strength.
$z(\mathbf{r})$	Surface topography (height) as a function of position.
$z_0(\mathbf{r})$	Deterministic large-scale roughness.
$Z(\mathbf{k})$	Wavenumber (k-space) representation of the surface.
$<z>$	Mean surface height.

[1] A. G. Voronovitch, "Small slope approximation in the theory of wave scattering at rough surfaces," Zh. Eksp. Teor. Fiz. **89**, 116–125 (1985).

[2] R. F. Gragg, D. Wurmser, and R. C. Gauss, "Small-slope scattering from rough elastic ocean floors: General theory and computational algorithm," J. Acoust. Soc. Am. **110**, 2878–2901 (2001).

[3] W. A. Kinney, C. S. Clay, and G. A. Sandness, "Scattering from a corrugated surface: Comparison between experiment, Helmhotz-Kirchhoff theory, and the facet-ensemble method," J. Acoust. Soc. Am. **73**, 183–194 (1983).

[4] R. S. Keiffer and J. C. Novarini, "A wedge assemblage method for 3-D acoustic scattering from sea surfaces: Comparison with a Helmholtz-Kirchhoff method," in *Computational Acoustics*, edited by D. Lee, A. Cakmak, and R. Vichnevetsky (Elsevier, Amsterdam, 1990), pp. 67–81.

[5] J. G. Zornig, "Physical modeling of underwater acoustics," in *Ocean Acoustics*, edited by J. A. DeSanto (Springer-Verlag, New York, 1979), Chap. 4, pp. 159–186.

[6] B. B. Mandelbrot, *The Fractal Geometry of Nature* (W. H. Freeman, New York, 1983).

[7] J. A. Ogilvy, *Theory of Wave Scattering from Random Rough Surfaces* (Adam Hilger, New York, 1991).

[8] L. E. Gilbert and A. Malinverno, "A characterization of the spectral density of residual ocean floor topography," Geophys. Res. Lett. **15**, 1401–1404 (1988).

[9] N. S. Neidell, "Spectral studies of marine geophysical profiles," Geophys. **31**, 122–134 (1966).

[10] T. H. Bell Jr., "Statistical features of sea-floor topography," Deep-Sea Res. **22**, 883–892 (1975).

[11] R. S. Sayles and T. R. Thomas, "Surface topography as a nonstationary random process," Nature **271**, 431–434 (1978).

[12] J. M. Berkson and J. E. Matthews, "Statistical properties of seafloor roughness," in *Acoustics of the Sea-Bed*, edited by N. G. Pace (Bath Univ. Press, Bath, Eng., 1983), pp. 215–223.

[13] C. G. Fox and D. E. Hayes, "Quantitative methods for analyzing the roughness of the seafloor," Rev. Geophys. **23**, 1–48 (1985).

[14] A. Malinverno, "Segmentation of topographic profiles of the seafloor based on a self-affine model," IEEE J. Oceanic Eng. **14**, 348–359 (1989).

[15] J. M. Bergin, "Analytical and physical aspects of two-dimensional spectra associated with stationary random processes," NRL/FR/8995, U. S. Naval Research Laboratory, Washington, D.C., August, 1986.

[16] M. V. Berry, "Diffractals," J. Phys. A **12**, 781–797 (1979).

[17] K. B. Briggs, "Microtopographical roughness of shallow-water continental shelves," IEEE J. Oceanic Eng. **14**, 360–367 (1989).

[18] J. A. Goff and T. H. Jordan, "Stochastic modeling of seafloor morphology: Inversion of Sea Beam data for second-order statistics," J. Geophys. Res. **93**, 13589–13608 (1988).

[19] R. Kant, "Statistics of approximately self-affine fractals: Random corrugated surface and time series," Phys. Rev. E **53**, 5749–5763 (1996).

[20] E. L. Church, "Fractal surface finish," Appl. Opt. **27**, 1518–1526 (1988).

[21] J. E. Moe and D. R. Jackson, "Near-field scattering through and from a two-dimensional fluid-fluid rough interface," J. Acoust. Soc. Am. **103**, 275–287 (1998).

[22] R. Dashen, F. S. Henyey, and D. Wurmser, "Calculations of acoustic scattering from the ocean surface," J. Acoust. Soc. Am. **88**, 310–323 (1990).

[23] D. Wurmser, "Stochastic cross-sections based on the small slope approximation: Theory," NRL/MR/7140–05–8816, U. S. Naval Research Laboratory, Washington, D.C., January, 2005.

[24] S. R. Brown and C. H. Scholz, "Broad bandwidth study of the topography of natural rock surfaces," J. Geophys. Res. **90**, 12575–12582 (1985).

[25] U. C. Herzfeld and C. Overbeck, "Analysis and simulation of scale-dependent fractal surfaces with application to seafloor morphology," Comp. Geosci. **25**, 979–1007 (1999).

[26] K. Briggs, D. Tang, and K. Williams, "Characterization of interface roughness of rippled sand off Fort Walton Beach, Florida," IEEE J. Oceanic Eng. **27**, 505–514 (2002).

[27] A. Ivakin, "Mechanisms of seafloor scattering: Roughness vs discrete inclusions," J. Acoust. Soc. Am. **116**, 2575 (A) (2004), presented at the 148th meeting of the Acoustical Society of America, 15-19 November 2004, paper 3aUW1.

[28] B. B. Mandelbrot, *Fractals: Form, Chance, and Dimension* (Freeman, San Francisco, 1977).

[29] B. B. Mandelbrot and J. W. Van Ness, "Fractional Brownian motions, fractional noises, and applications," SIAM Rev. **10**, 422–437 (1968).

[30] G. A. Hunt, "Random Fourier transforms," Trans. Amer. Math. Soc. **71**, 38–69 (1951).

[31] M. S. Taqqu, "Fractional Brownian motion and long-range dependence," in *Theory and applications of long-range dependence*, edited by P. Doukhan, G. Oppenheim, and M. S. Taqqu (Birkhäuser, Boston, 2003), pp. 5–38.

[32] J. Feder, *Fractals* (Plenum Press, New York, 1988).

[33] N. P. Greis and H. S. Greenside, "Implication of a power-law power-spectrum for self-affinity," Phys. Rev. A **44**, 2324–2334 (1991).

[34] D. J. Whitehouse and J. F. Archard, "The properties of random surfaces of significance in their contact," Proc. R. Soc. **A316**, 97—121 (1970).

[35] "Fractal and surface roughness," *Metrology and Properties of Engineering Surfaces*, edited by E. Mainsah, J. A. Greenwood, and D. G. Chetwynd (Kluwer, Boston, 2001), pp. 33–41.

[36] S. Gautier and D. Gibert, "Scattering from a fractal surface: acoustical experiments and comparison with near-nadir models," Icarus **167**, 453–463 (2004).

[37] B. B. Mandelbrot, "Self-affine fractals and fractal dimension," Phys. Scrip. **32**, 257–260 (1985).

[38] T. Gneiting and M. Schlather, "Stochastic models that seperate fractal dimension and the Hurst effect," SIAM Rev. **46**, 269–282 (2004).

[39] G. H. Hardy, "Weierstrass's non-differentiable function," Tr. Am. Math. Soc. **17**, 301–325 (1916).

[40] M. V. Berry and J. H. Hannay, "Topography of random surfaces," Nature **273**, 573 (1978).

[41] P. Flandrin, "On the spectrum of fractional Brownian motion," IEEE Trans. Inf. Theory **35**, 197–199 (1989).

[42] P. Flandrin, "Wavelet analysis and synthesis of fractional Brownian motion," IEEE Trans. Inf. Theory **38**, 910–917 (1992).

[43] S. Orey, "Gaussian sample functions and Haussdorff dimension of level crossings," Z. Wahrscheinlichkeitstheor. **15**, 249–256 (1970).

[44] S. E. Hough, "On the use of spectral methods for the determination of fractal dimension," Geophys. Res. Lett. **16**, 673–676 (1989).

[45] O. I. Yordanov and K. Ivanova, "Description of surface roughness as an approximate self-affine random structure," Surf. Sci. **331–333**, 1043–1049 (1995).

[46] D. T. Hristopulos, "Permissibility of fractal exponents and models of band-limited two-point functions for fGn and fBm random fields," Stoch. Environ. Res. Risk Assess. **17**, 191–216 (2003).

[47] J. C. Russ, *Fractal Surfaces* (Plenum Press, New York, 1994).

[48] G. Franceschetti, A. Iodice, M. Migliaccio, and D. Riccio, "Fractals and the small perturbation scattering model," Radio Sci. **34**, 1043–1054 (1999).

[49] B. Dubuc, J. F. Quiniou, C. Roques-Carmes, C. Tricot, and S. W. Zucker, "Evaluating the fractal dimension of profiles," Phys. Rev. A **39**, 1500–1513 (1989).

[50] O. I. Yordanov and N. I. Nickolaev, "Self-affinity of time series with finite domain power-law power spectrum," Phys. Rev. E **49**, R2517–R2520 (1994).

[51] J.-S. Leu, "On estimating the spectral exponent of fractional Brownian motion," IEEE Trans. Inf. Theory **41**, 233–244 (1995).

[52] A. R. Mehrabi, H. Rassamdana, and M. Sahimi, "Characterization of long-range correlations in complex distributions and profiles," Phys. Rev. E **56**, 712–722 (1997).

[53] C. Castelnovo, A. Podestà, P. Piseri, and P. Milani, "Fractal analysis of sampled profiles: Systematic study," Phys. Rev. E **65**, 021601 (2002).

[54] O. I. Yordanov and I. S. Atansov, "Self-affine random surfaces," Eur. Phys. J. B **29**, 211–215 (2002).

[55] "Measuring surfaces," *Metrology and Properties of Engineering Surfaces*, edited by E. Mainsah, J. A. Greewood, and D. G. Chetwynd (Kluwer, Boston, 2001), pp. 59–66.

[56] R. J. Soukup and R. F. Gragg, "Backscatter from a limestone seafloor at 2-3.5 kHz: Measurements and modeling," J. Acoust. Soc. Am. **113**, 2501–2514 (2003).

[57] R. J. Soukup, R. F. Gragg, R. W. Wiley, and B. Inanli, "Rough surface scattering from an elastic scale model of an ocean bottom," J. Acoust. Soc. Am. **114**, 2311 (A) (2003), presented at the 146th meeting of the Acoustical Society of America, 10-14 November 2003, paper 1pUW2.

[58] M. V. Berry and Z. V. Lewis, "On the Weierstrass-Mandelbrot fractal function," Proc. R. Soc. Lond. A **370**, 459–484 (1980).

[59] K. Weierstrass, Über continuirliche Functionen eines reellen Arguments, die für keinen Werth des letzteren einen bestimmten Differentialquotienten besitzen (Concerning a continuous function of real arguments that is nowhere differentiable), presented to the Berlin Academy (1872), first published in Ref. 60.

[60] K. Weierstrass, in *Mathematische Werke* (Mayer & Muller, Berlin, 1895–), Vol. 2, pp. 71–74.

[61] B. R. Hunt, "The Hausdorff dimension of graphs of Weierstrass functions," Proc. Am. Math. Soc. **126**, 791–800 (1998).

[62] H. M. Hastings and G. Sugihara, *Fractals: A User's Guide for the Natural Sciences* (Oxford University Press, New York, 1993).

[63] S. Kumar and G. S. Bodvarsson, "Fractal study and simulation of fracture roughness," Geophys. Res. Lett. **17**(6), 701–704 (1990).

[64] A. G. Garcia, "Orthogonal sampling formulas: A unified approach," SIAM Rev. **42**, 499–512 (2000).

[65] J. S. Lim, *Two-Dimensional Signal and Image Processing* (Prentice-Hall, Englewood Cliffs, New Jersey, 1990).

[66] E. I. Thorsos, "The validity of the Kirchhoff approximation for rough surface scattering using a Gaussian roughness spectrum," J. Acoust. Soc. Am. **83**, 78–92 (1988).

[67] H. Stark and J. W. Woods, *Probability and Random Processes with Applications to Signal Processing*, 3rd ed. (Prentice-Hall, Upper Saddle River, New Jersey, 2002).

[68] J.-J. Sung, G.-S. Kang, and S. Kim, "A transient noise model for frequency-dependent noise sources," IEEE Trans. Computer-Aided Design Integrated Circuits Systems **22**, 1097–1104 (2003).

[69] J. M. Proud Jr., R. T. Beyer, and P. Tamarkin, "Reflection of sound from randomly rough surfaces," J. Appl. Phys. **31**, 543–552 (1960).

[70] C. W. Horton, Sr., S. K. Mitchell, and G. R. Barnard, "Model studies on the scattering of acoustic waves from a rough surface," J. Acoust. Soc. Am. **41**, 635–643 (67).

[71] G. R. Mellema, "Subcritical acoustic scattering across a rough fluid-solid interface," Ph.D. thesis, Department of Electrical Engineering, University of Washington, 1999.

[72] P. Bourke, Computer based terrain visualization: From points to wood, `http://astronomy.swin.edu.au/~pbourke/terrain/terrainvis/`, 1993.

[73] Y. Kuga and P. Phu, "Experimental studies of millimeter-wave scattering in discrete random media and from random surfaces," Prog. Electromag. Res. (PIER) **14**, 37–88 (1996).

[74] A. Warkentin, P. Hoskins, F. Ismail, and S. Bedi, "Computer aided 5-axis machining," in *Systems Techniques and Computational Methods*, edited by C. Leondes (CRC Press, Washington, D.C., 2001).

[75] Z. Dong, H. Li, and G. W. Vickers, "Optimal rough machining of sculptured parts on a CNC milling machine," J. Eng. Ind. - Trans. Am. Soc. Mech. Eng. **115**, 424–431 (1993).

[76] T. R. Thomas, "Measurement," in *Rough Surfaces*, edited by T. R. Thomas (Longman, New York, 1982), Chap. 2–3, pp. 11–69.

[77] F. M. M. Chan, E. J. Davis, T. G. King, and K. J. Stout, "Some performance aspects of a multi-axis touch trigger probe," Meas. Sci. Technol. **8**, 837–848 (1997).

[78] W. T. Estler, S. D. Phillips, B. Borchardt, T. Hopp, M. Levenson, K. Eberhardt, M. McClain, Y. Shen, and X. Zhang, "Practical aspects of touch-trigger probe error compensation," Precis. Eng. **21**, 1–17 (1997).

[79] C. Dong, C. Zhang, B. Wang, and G. Zhang, "Prediction and compensation of dynamic errors for coordinate measuring machines," J. Manufac. Sci. Eng.-Trans. ASME **124**, 509–514 (2002).

[80] J.-J. Wu, "Spectral analysis for the effect of stylus tip curvature on measuring rough profiles," Wear **230**, 194–200 (1999).

[81] J.-J. Wu, "Spectral analysis for the effects of stylus tip curvature on measuring isotropic rough surfaces," Measur. Sci. Tech. **13**, 720–730 (2002).

[82] S. M. Kay, *Modern Spectral Estimation: Theory and Application* (Prentice Hall, Englewood Cliffs, New Jersey, 1988).

[83] R. T. Austin, A. W. England, and G. H. Wakefield, "Special problems in the estimation of power-law spectra as applied to topographical modeling," IEEE Trans. Geosci. Remote Sens. **32**, 928–939 (1994).

[84] The increments process of Brownian motion is Gaussian noise, which has a perfectly white PSD and therefore has an autocorrelation function that is a delta function.